12

# Turbulent Flow Around Submerged Bendway Weirs and Its Influence on Channel Navigation

Yafei Jia[1], Tingting Zhu[1] and Steve Scott[2]
[1]*The University of Mississippi*
[2]*US Army ERDC Waterways Experiment Station*
*United States*

## 1. Introduction

Flow in curved channel bends is typically characterized by helical secondary currents (HSC) which play an important role in redistributing the momentum of river flow in a cross-section, resulting in lateral sediment transport, bank erosion and channel migration. Secondary current introduces difficulties for channel navigation because it tends to force barges toward the outer bank. Submerged weirs (SWs) are engineering structures designed to improve navigability of bendways. They have been constructed along many bends of the Mississippi River for improving barge navigation through these bends (Davinroy & Redington, 1996). Because of the complexity of channel morphology and flow conditions, not all the installed SWs were effective as expected (Waterway Simulation Technology, Inc., 1999). It is necessary, therefore, to study the turbulent flow field around submerged weirs and the mechanisms affect navigation.

The HSCs can be computed analytically if the channel form and cross-section can be approximated as circular and rectangular (Rozovskii, 1961). Curved channel flows can be simulated by depth averaged models. Although the main flow distribution can be predicted quite satisfactorily using two-dimensional (2D) models (Jia et al., 2002a; Jin & Steffler, 1993), the secondary flow resulting from hydraulic structures is difficult to simulate with these models. The approach of embedding an analytical solution (Hsieh and Yang, 2003) or three-dimensional (3D) simulation results (Duan et al., 2001) into a 2D model may not be appropriate when submerged weir(s) are present. Compared with two-dimensional models, three-dimensional models are more suitable and have been widely used for open channel flow simulations particularly for flows in curved channels. From early research by Leschziner & Rodi (1979) to the growing popularity of applications by Jia & Wang (1992), Wu et al. (2000), Morvan et al. (2002), Wilson et al. (2003), Olson (2003) etc., three-dimensional numerical models have been proven to be capable of predicting general helical currents in curved channels. Wilson et al. (2003) solved a multiple-bend curved-channel flow problem using the $k$-$\varepsilon$ closure and rigid lid assumption with a finite volume code of non-orthogonal structured grid. Morvan et al. (2002) simulated flow in a meander channel with flood plains. Both the $k$-$\varepsilon$ closure and Reynolds stresses model were applied with a rigid lid. Olsen (2003) applied a 3D model with the $k$–$\varepsilon$ closure to simulate the channel meandering process. Natural river flow, sedimentation and bed change were computed by Wu et al. (2000) using a 3D model, with $k$-$\varepsilon$ closure used for the hydrodynamics

computation. Lai et al. (2003) simulated a curved channel in laboratory scale using a finite volume model of non-structured grid with a rigid lid and free slip boundary condition specified at the free surface. Although the general helical current can be simulated by using different turbulence closure schemes, the outer bank vortex cell, with its size being the order of the water depth (Blanckaert & Graf, 2001; De Vriend, 1979), could not be captured without considering the non-linearity of turbulence stresses. Jia et al. (2001a) and Wang et al. (2008) reported the simulation of curved channel flows using a nonlinear $k-\varepsilon$ closure. The non-linear model can predict secondary circulation near the water surface and outer bank in addition to the general helical current driven by channel curvature and gravity. A large eddy simulation (LES) model which could also simulate this vortex adequately was reported by Booij (2003).

The US Corps of Engineers (Davinroy & Redington, 1996) determined that one practical option for improving navigation through bendways is to install submerged weirs (dikes) that project from the outer bank into the channel and are oriented upstream. Pilots operating barge vessels on the river reported that the submerged weirs, placed across the channel thalweg and angled upstream, realigned the flow away from the outer bank to the middle of the channel, thus allowing more room for maneuvering through the bend. From 1989 to 1995, there were 114 submerged weirs constructed in 13 bends of the Mississippi River (Davinroy & Redington, 1996). However, not all the submerged weirs yielded satisfactory results (Waterway Simulation Technology, 2002). Apparently, the impact of these submerged weirs on bendway hydrodynamics and their effectiveness on channel navigation are not well understood.

Submerged weirs (SW) can realign general channel flow distribution because of their obstruction to approaching flow. Kinzli and Thornton (2010) developed empirical equations for eddy velocities in bendway weir fields using a rigid bed physical model. Three design parameters were tested: weir spacing, length and orientation angle. Jarrahzade and Bejestan (2011) conducted experiments to study the local scour depths around the submerged weirs installed at the outer bank of a bendway in the laboratory flume. Hydraulic structures similar to submerged weirs (such as spur dikes) have been studied using numerical simulations (Jia & Wang, 1993; Ouillon & Dartus, 1997) for various purposes. Jia & Wang (1993) applied 3D free surface models to simulate flows around hydraulic structures such as spur dikes; numerical solutions of velocity field and shear stress on the bed agreed with those observed (Rajaratnam & Nwachukwu, 1983). Submerged vanes (Odgaard & Kennedy, 1983) were introduced in bendways to reduce the strength of helical current. For preventing bank erosion of a curved channel reach, Bhuiyan & Hey (2001) studied a J-vane installed near the outer bank with a sharp angle to the bank line. Olsen & Stokseth (1995) computed a 3D flow in a short channel with large rocks. A porosity model was used to handle the rock elements which were comparable to mesh sizes. Bhuiyan & Olsen (2002) studied local scouring process around a dike with a 3D model; reattachment length and shear stress distribution on the bed prior to scouring were used to test mesh sensitivity and validate the model qualitatively. Jia et al. (2005) studied the turbulent flow around a submerged weir in a curved channel using a 3D model. The computational model was also applied to study the flow in a reach of the Mississippi River with a weir field (Jia et al., 2009). Martin & Luong (2010) applied a 3D curvilinear hydrodynamics and sediment (CH3D-SED) model to a river reach of Atchafalaya River at Morgan City, LA. Several design alternatives of multiple submerged weirs were simulated and the favorable options were identified to reduce shoaling and dredging.

In this chapter, computational studies of the channel flow affected by SWs are introduced. A finite element based three-dimensional numerical, CCHE3D, was used to study HSC and the

flow distribution around submerged weirs. The computational model has been validated using physical experiment data collected by the US Army Corps of Engineers. The numerical simulations indicated that the submerged weirs significantly altered the general HSC. Its presence induced a skewed pressure difference across its top and a triangular-shaped recirculation to the downstream side. The overtopping flow tends to realign toward the inner bank and therefore improves conditions for navigation. Validated by physical experiment data, this numerical model was applied to a field scale study of hydrodynamics in the Victoria Bendway in the Mississippi River. 3D flow field data were also used to validate this model with good agreement. The simulated flow realignment near the free surface indicates that the flow conditions in the bendway were improved by the submerged weirs; however, the effectiveness of each weir depends on its alignment, local channel morphology, flow and sediment transport conditions.

## 2. Numerical model – CCHE3D

The CCHE3D model developed at the National Center for Computational Hydroscience and Engineering is a three-dimensional finite element based, numerical simulation model for unsteady free surface turbulent flows, and it is capable of handling flows and sediment transport in complex channel domains and irregular bed topography. The model solves unsteady three-dimensional Reynolds equations using the Efficient Element Method based on the collocation approach (Mayerle et al., 1995; Wang & Hu, 1992). The CCHE3D model has been verified by analytical methods and validated using many sets of data from physical experiments, including simulation of near field flows around hydraulic structures like bridge piers, abutments, spur dikes, submerged dikes and submerged weirs (Jia & Wang, 2000a, 2000b; Jia et al., 2005; Kuhnle et al.; 2002).

### 2.1 Governing equations

The unsteady, three-dimensional Reynolds-averaged momentum equations and continuity equation are solved in the CCHE3D model

$$\frac{\partial u_i}{\partial t} + u_j \frac{\partial u_i}{\partial x_j} = -\frac{1}{\rho}\frac{\partial p}{\partial x_i} + \frac{\partial}{\partial x_j}\left(\nu \frac{\partial u_i}{\partial x_j} - \overline{u_i' u_j'}\right) + f_i \tag{1}$$

$$\frac{\partial u_i}{\partial x_i} = 0 \tag{2}$$

where $u_i$ ($i$=1,2,3) represent the Reynolds-averaged flow velocities ($u$, $v$, $w$) in Cartesian coordinate system ($x$, $y$, $z$), $u_i'$ is velocity fluctuation, $-\overline{u_i' u_j'}$ are the Reynolds stresses, $u_i$ represent the mean behavior of the flow over a time scale much larger than that for $u_i'$, $p$(=$p_h$+ $p_d$ ) is pressure with $p_h$ being hydrostatic and $p_d$ non-hydrostatic pressure, $\rho$ is the fluid density, $\nu$ is the fluid kinematic viscosity and $f_i$ are body force terms. The motion of free surface is computed using the free surface kinematics equation:

$$\frac{\partial S}{\partial t} + u_s \frac{\partial S}{\partial x} + v_s \frac{\partial S}{\partial y} - w_s = 0 \tag{3}$$

where $S$ and the subscript, $s$, denote the free surface elevation and velocity components at the surface, respectively. Because free surface elevation determines the hydrostatic pressure distribution, $p_h = g(S - z)$, the main driving force of open channel flows, it is one of the key variables in this study. The non-hydrostatic pressure was solved by using velocity correction method on a staggered grid and applied to enforcing the computed flow to satisfy the divergence free condition (Jia et al., 2001b). In the application to the turbulence flow around submerged weirs, due to the strong three-dimensionality of the flow near the weirs, the non-hydrostatic pressure was computed and applied.

### 2.2 Turbulence closure model

There are six turbulence closure models included: constant, parabolic and mixing length eddy viscosity models, and standard, RNG and non-linear $\kappa$–$\varepsilon$ two equation models (Speziale, 1987). Considering that the transport of turbulence is significant with the presence of submerged weirs, two-equation models are applicable. As the non-linear $k$–$\varepsilon$ model requires high grid density to resolve the secondary flow structures driven by turbulence normal stresses (Jia et al., 2001a), and the problem concerned in this study is shear dominated, the non-linear closure was not selected. For this particular application the standard $\kappa$–$\varepsilon$ turbulence closure was used:

$$\frac{\partial k}{\partial t} + u_j \frac{\partial k}{\partial x_j} - \frac{\partial}{\partial x_j}\left(\frac{\nu_t}{\sigma_k}\frac{\partial k}{\partial x_j}\right) = P - \varepsilon \tag{4}$$

$$\frac{\partial \varepsilon}{\partial t} + u_j \frac{\partial \varepsilon}{\partial x_j} - \frac{\partial}{\partial x_j}\left(\frac{\nu_t}{\sigma_\varepsilon}\frac{\partial \varepsilon}{\partial x_j}\right) = c_{\varepsilon 1} P \frac{\varepsilon}{k} - c_{\varepsilon 2}\frac{\varepsilon^2}{k} \tag{5}$$

where $k$ represents the turbulent kinetic energy $\overline{u_i' u_i'}/2$, $\varepsilon$ represents the rate of dissipation of turbulent kinetic energy, $\nu_t$ denotes the turbulent viscosity given by:

$$\nu_t = c_\mu \frac{k^2}{\varepsilon} \tag{6}$$

and $P$ is the production of turbulent kinetic energy computed from:

$$P = \nu_t \left(\frac{\partial u_i}{\partial x_j} + \frac{\partial u_j}{\partial x_i}\right)\frac{\partial u_i}{\partial x_j} \tag{7}$$

Standard values of coefficients appearing in the preceding equations were assigned: $c_\mu$=0.09, $\sigma_\kappa$=1.0, $\sigma_\varepsilon$=1.3, $c_{\varepsilon 1}$=1.44, $c_{\varepsilon 2}$=1.92. It is well known that by using this closure scheme, the prediction of recirculation length behind an obstacle or a step in straight channels may be somewhat shorter than those measured. This closure scheme is acceptable in the investigation of flows around submerged weirs as the overall flow pattern and structure around the weir were more of a concern to the study than the exact length of the recirculation. A structured 3D grid was used with each finite element formed by a hexahedron (Fig. 1). The local space coordinates, ($\xi$, $\eta$, $\zeta$), are transformed to the global Cartesian coordinate in a way analogous to the 2D case (Jia & Wang, 1999). All of the 3D first-order non-convective and second order operators are constructed using this 1D quadratic interpolation function.

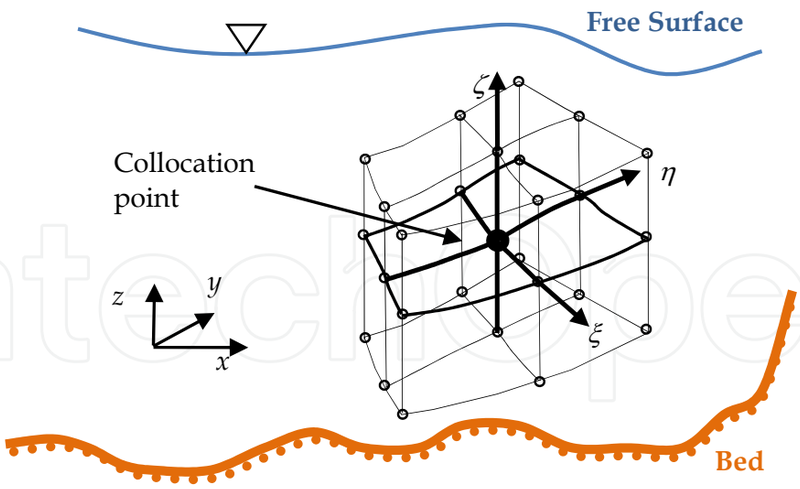


Fig. 1. Sketch of 3D element configuration in physical space

### 2.3 Boundary conditions

Measured steady water stage and flow discharge were used as the downstream and upstream boundary conditions. The turbulence energy, $k$, at the inlet was approximated by using the formula proposed by Nezu & Nakagawa (1993) and the rate of energy dissipation, $\varepsilon$, was computed by $k$ and the assumption of parabolic turbulent eddy viscosity distribution for uniform flows. The wall function was specified for the wall boundaries such as the channel bed and the submerged weirs with different roughness, and the turbulence energy and dissipation were assumed to be in local equilibrium. Due to the near parabolic shape of the channel cross-section, the water depth along the water edge near the bank line was zero. A very small flow depth was set for the boundary mesh lines and the $k$ and $\varepsilon$ values for uniform flow were specified for the $k$-$\varepsilon$ model.

### 2.4 Upwinding scheme

To eliminate oscillations due to advection, upwinding was introduced via a unique convective interpolation function, which takes into account the local flow direction and emphasizes the upstream influence. It is applied to compute advection terms in the momentum equations (1), the convection terms in the free surface kinematics equation (3) and those in the turbulence transport equations (4, 5). This convective interpolation function was obtained by solving a linear and steady convection-diffusion equation analytically over a one-dimensional local element:

$$c_1 = \frac{1}{2T}\left[(2e^{p_e\xi} - e^{-p_e} - e^{p_e})\left(1 - \frac{\xi_0(R+1)}{\xi_0 R+1}\right) + T - \frac{\xi T(R+1)}{\xi_0 R+1}\right] \tag{8a}$$

$$c_2 = 1 - c_1 - c_3 \tag{8b}$$

$$c_3 = \frac{1}{2T}\left[(2e^{p_e\xi} - e^{-p_e} - e^{p_e})\left(1 - \frac{\xi_0(R-1)}{\xi_0 R+1}\right) + T - \frac{\xi T(R-1)}{\xi_0 R+1}\right] \tag{8c}$$

$$T = e^{p_e} + e^{-p_e} - 2e^{p_e \xi_o} \tag{9a}$$

$$R = (e^{p_e} - e^{-p_e}) / T \tag{9b}$$

$$p_e = u_c / v_t \tag{9c}$$

where $u_c$ is the flow velocity at the collocation node in the direction of the local coordinate $\xi$. Upwinding is adjusted by the local *Peclet* number $p_e = u_c / v_t$ (the length scale of the local element is $\xi \pm = 1.0$). The limiting scheme to $p_e$ (Jia & Wang, 1999) was applied to minimize the numerical diffusion. This convective interpolation function is applied to all three directions locally. Gradients of velocities and other transport variables in the local directions are computed analytically. The convective operators thus obtained are then transformed to the Cartesian coordinate system via

$$\begin{pmatrix} \frac{\partial}{\partial x} \\ \frac{\partial}{\partial y} \\ \frac{\partial}{\partial z} \end{pmatrix} = \begin{vmatrix} \frac{\partial y}{\partial \eta}\frac{1}{D}, & -\frac{\partial y}{\partial \xi}\frac{1}{D}, & -\frac{\left(\frac{\partial y}{\partial \eta}\frac{\partial z}{\partial \xi} - \frac{\partial y}{\partial \xi}\frac{\partial z}{\partial \eta}\right)}{D\frac{\partial z}{\partial \zeta}} \\ -\frac{\partial x}{\partial \eta}\frac{1}{D}, & \frac{\partial x}{\partial \xi}\frac{1}{D}, & -\frac{\left(-\frac{\partial x}{\partial \eta}\frac{\partial z}{\partial \xi} + \frac{\partial x}{\partial \xi}\frac{\partial z}{\partial \eta}\right)}{D\frac{\partial z}{\partial \zeta}} \\ 0, & 0, & \frac{1}{\frac{\partial z}{\partial \zeta}} \end{vmatrix} \cdot \begin{pmatrix} \frac{\partial}{\partial \xi} \\ \frac{\partial}{\partial \eta} \\ \frac{\partial}{\partial \zeta} \end{pmatrix} \tag{10a}$$

$$D = -\frac{\partial x}{\partial \eta}\frac{\partial y}{\partial \xi} + \frac{\partial x}{\partial \xi}\frac{\partial y}{\partial \eta} \tag{10b}$$

Eq. 10 transforms operators for the element (Fig. 1) with the local coordinate $\zeta$ in the vertical ($z$) direction.

Eq. 10a & 10b indicate that vertical distributions of horizontal velocities are used to compute terms as part of $\partial / \partial x$ and $\partial / \partial y$ when mesh surface of $\xi$–$\eta$ plan is inclined, creating a vertical convective term. Although there are other options of upwinding schemes in the CCHE3D model such as a second order upwinding and the QUICK scheme, the convective interpolation function was selected in this study due to its simplicity for the implicit time marching scheme: it requires only three nodes in each direction of the mesh lines; and some level of numerical diffusion is not so critical as in the case of jet impinging flow simulation (Jia et al., 2001b). A verification test of this scheme using a 3D manufactured analytical solution indicated that this scheme is about 1.6 order of accuracy (Wang et al., 2008). Wilson et al. (2003) tested that a second order upwinding scheme improved the helical flow computation by less than five percent. The system of equations is solved implicitly by using the Strongly Implicit Procedure (Stone, 1968) with the Euler's time marching scheme.

The CCHE3D model has been validated using physical model and field data. For this particular study, a physical experiment and a field case, Victorial Bendway of the Mississippi River, were also used for validation. The comparison between the simulated and measured flow field, the secondary flow field around the structures, and the impacts of weirs on the flow field will be presented.

## 3. Model validation using physical experiment

### 3.1 Physical model

Computational model validation was performed based on flow data measured in the physical model study conducted at Coastal and Hydraulic Laboratory of Engineer Research and Development Center (ERDC), US Army Corps of Engineers, Waterways Experimental Station, Vicksburg, Mississippi. Velocity data measured with an ADVP device were used to validate the computed flow field. To speed up the computations, CCHE2D (Jia et al., 2002a) was used to simulate the flow in the entire experimental channel. Using the boundary conditions provided by the 2D model, a shorter reach in the bendway that contained the submerged weir was then simulated with the 3D model. The effective roughness heights of the channel were obtained by calibration using the measured water surface elevation along the channel. This roughness was used for the 3D simulation with the exception of the surface roughness of the SW. The channel plan form, cross sectional form, the location of the submerged weir and the 2D and 3D simulation domains are shown in Fig. 2.

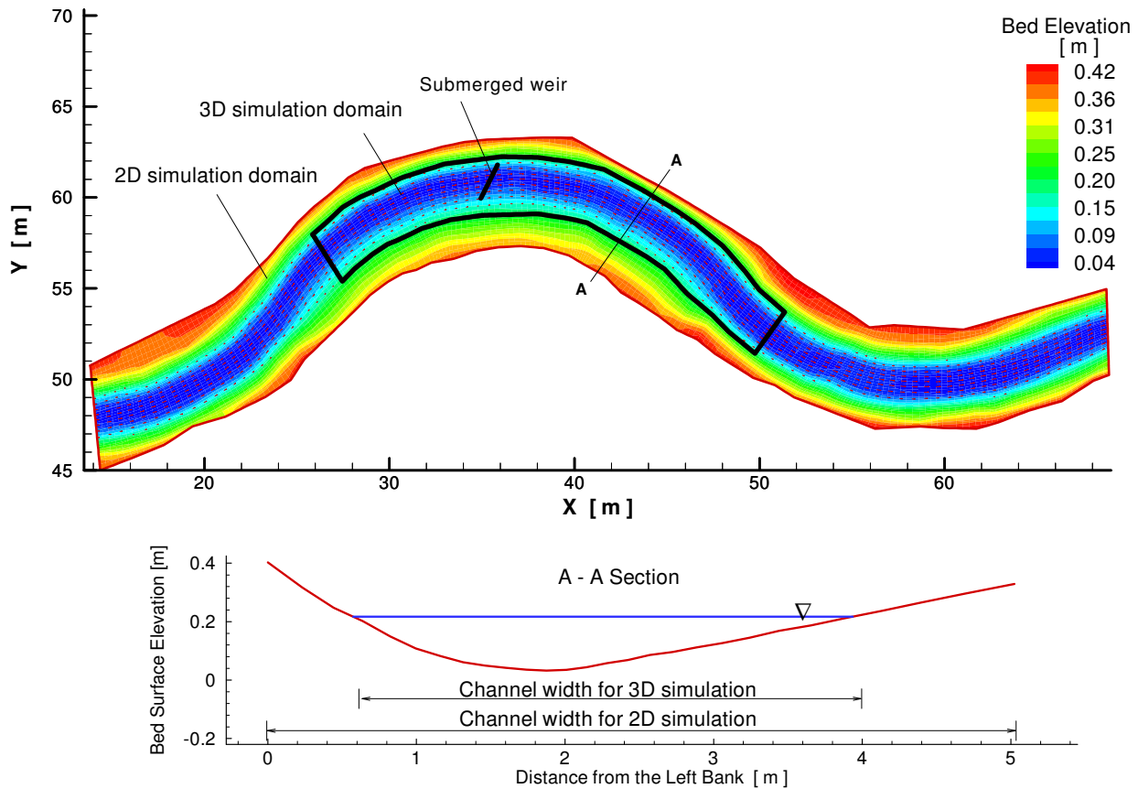


Fig. 2. Physical model set up and numerical simulation domain

Table 1 presents two flow conditions for the single submerged weir design tests; both were used for experiments with and without this submerged weir. The weir was made of approximately 2 cm size gravel and installed in the channel bend apex, attaching to the outer bank angled 20˚ upstream with a flow depth (clearance) of 9.5 cm. The shape of the weir was a trapezoid with a top width of 4 cm and a base width of 32 cm. The channel bed surface was of fine sand (median size: 0.43 mm). The effective channel bed roughness was a model parameter obtained by calibration. The flow velocity was mild ($Re$<2.8x10$^4$, $Fr$<0.25) to avoid erosion and entrainment of the loose bed material. Since the governing equations are time-dependent and the cases of this study are of steady state, simulations were terminated when the maximum incremental variation of solutions of each variable ($u_i$ , $S$, $k$ and $\varepsilon$) in the entire computational domain became small ($10^{-4}$~$10^{-5}$). When a steady state is reached, the flow discharge along the channel approaches to a constant: MAX [|$Q_{cs}$-Q|/Q] <0.01 ($Q_{cs}$ is the discharge through a cross-section).

| | Discharge $Q$ ($m^3/s$) | Mean Velocity, $U$ (m/s) | Effective bed roughness height, $k_s$ (m) | Roughness of submerged weir (m) | Width $W$ (m) | Reynolds number, $R_e$ | Froude number , $F_r$ |
|---|---|---|---|---|---|---|---|
| Run1 | 0.0413 | 0.125 | 0.005 | 0.02 | 3.1 | 13,250 | 0.123 |
| Run2 | 0.0851 | 0.252 | 0.008 | 0.02 | 3.17 | 27,700 | 0.248 |

Table 1. Flow conditions for the physical models Radius of curvature $R$=15.24m, Weir length $L$=1.8m, Weir angle $\alpha$=20$^o$, maximum depth $H_m$=0.182m, clarence $H_c$=0.095m, average depth $H_a$=0.106m. Mean water depth was used to calculate Reynolds number and Froude number.

A mesh sensitivity test was conducted to determine if the computational mesh had sufficient density for the problem. Simulation results of three mesh resolutions ($I_{\max} \times J_{\max} \times K_{\max}$ = 45x142x11, 79x142x11 and 45x142x31, in transversal, longitudinal and vertical directions, respectively) were compared. These meshes were designed to have much higher nodal density near the weir than that in the up and downstream part of the channel with smooth transitions. The second and the third mesh had a much higher number of nodes in the cross section and vertical direction. These extra mesh lines result in a higher element concentration around the weir and near the tip of the weir in particular. Simulations of the same flow scenario were conducted and the computational results compared to see if significant improvements were gained from the finer meshes. No significant difference was found in the near and far field of computed flows with the first two meshes. The third mesh results in more details in the recirculation zone, but no significant change in the flow in general. The validity of the first mesh for production runs was therefore confirmed.

### 3.2 Comparison of the simulation results and the measurements

Fig. 3 shows the bed bathymetry of the channel near the bend apex. The channel thalweg is closer to the outer bank to which the weir shoulder is attached. The submerged weir of $\alpha$ = 20$^o$ and $L$= 1.8 m is clearly seen. The dot lines aligned parallel to the weir are measurement ranges. The ranges are numbered from upstream to downstream, with three ranges on the front side (upstream) and the remaining on the back or downstream side. The longitudinal spacing between the first and the second range, the third and fourth, and between the

seventh and those that follow were 0.3048 m. The spacing between the other ranges is 0.1524 m. The transversal spacing of points along range 1, 8, 9, and 10 is 0.3048 m, with a spacing of 0.1524 m for the rest of ranges. Velocity data were taken at three levels (0.2 *h*, 0.6 *h* from surface and close to bed) at each measuring location. The data were sufficient to study the general flow distributions.

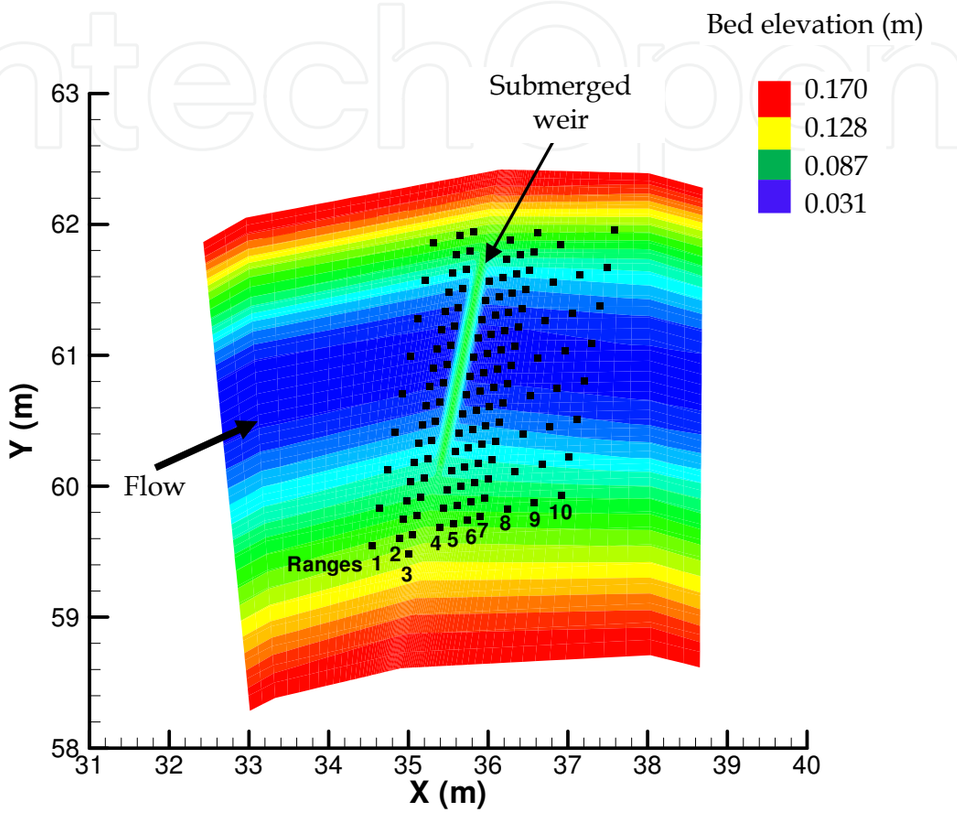


Fig. 3. Configuration of velocity measurement points around the submerged weir

Fig. 4a shows computed and measured velocity magnitude (Run2) along the 10 measurement ranges (transects) shown in Fig. 3. The velocities shown were measured at 20% of local flow depth (0.2 *h*) from the water surface. The horizontal axes are the distance from the left (outer) bank of the channel. The comparison of simulation and measurements for Run1 showed similar agreement in trend.

At Ranges 1, 2, and 3 located in front of the weir, the flow velocities were suppressed near the center part of the channel while the near bank velocities increase toward the weir. This was due to the high pressure resulting from the blockage of flow by the weir. This phenomenon was also evident for the velocity at the other levels (0.6 *h* and near bottom level). The increase of velocity near the tip of the weir in the physical model had resulted in some visible erosion or scouring of the bed. Ranges 4 through 10 were aligned behind the weir. Immediately downstream of the weir, the surface velocities were very high due to the pressure difference across the weir top (Section 4, 5, and 6). Because of the low pressure behind the weir, the velocities in further downstream sections were reduced, particularly in the center area. The

velocities near the bank were higher than those in the center part of the channel. The trend of decreasing velocity near the channel center line extends downstream beyond the last measuring section. Further downstream, the influence of the weir decreased and flow gradually recovered so that the maximum velocity re-appeared at the center of the channel.

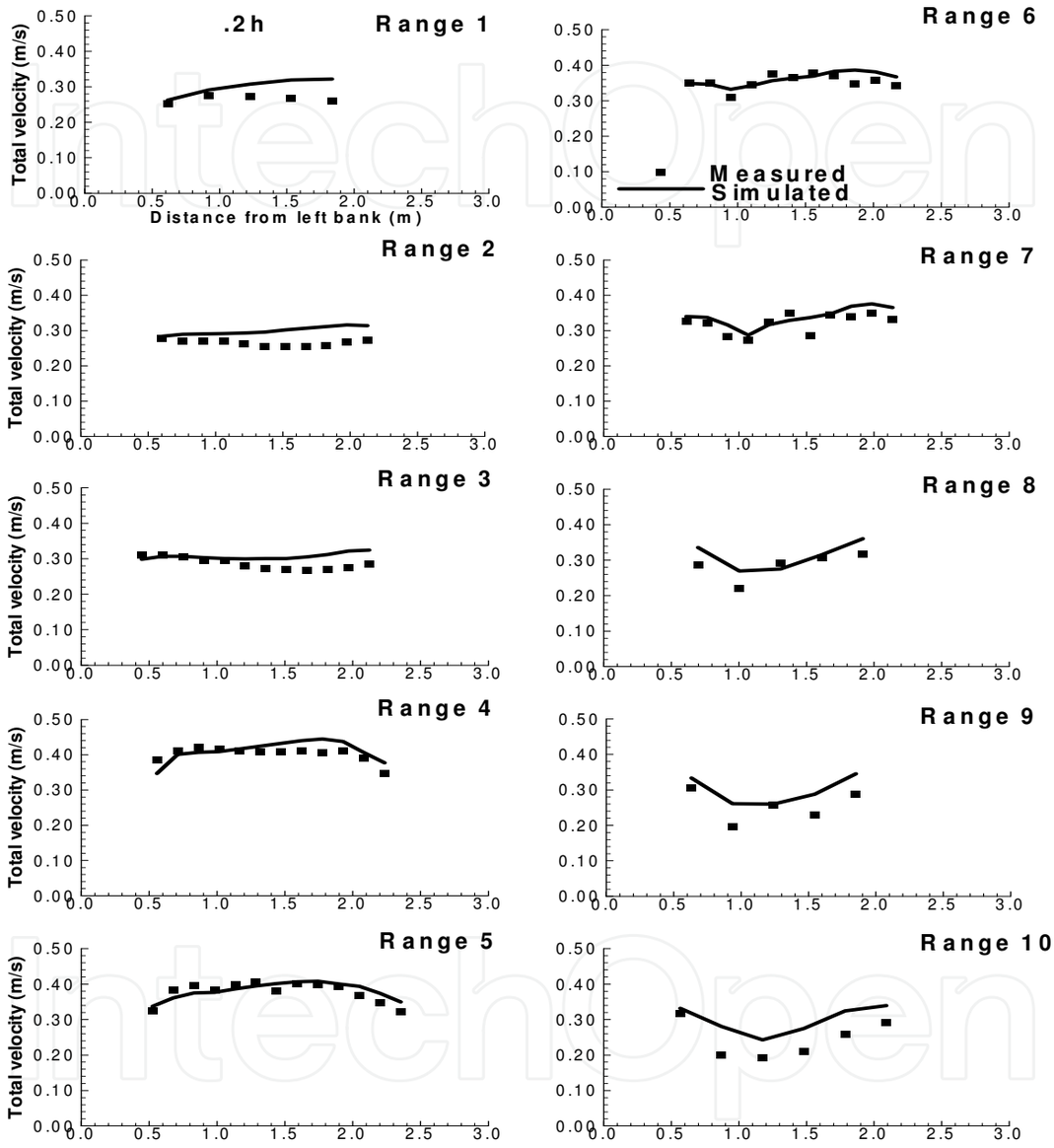


Fig. 4a. Comparison of simulated and measured total flow velocities at 0.2 *h* from the water surface around the submerged weir. Horizontal axis is the distance from the outer bank.

Fig. 4b shows the comparison of measured and computed velocities in these ten sections at the level 0.6 *h* from the water surface. The deceleration and separation of flow on the upstream side of the weir are more significant than those near surface. The trend that the flow accelerates along the streamlines near the banks is more pronounced. Downstream of the weir, the velocity decrease near the channel centerline is also more significant than the velocity decrease near the surface due to the existence of the recirculation flow. Since this

level is close to or cuts across the shear layer with a sharp angle where velocity varies rapidly in the vertical direction, the comparisons at this level on the downstream side have larger discrepancy than at other locations.

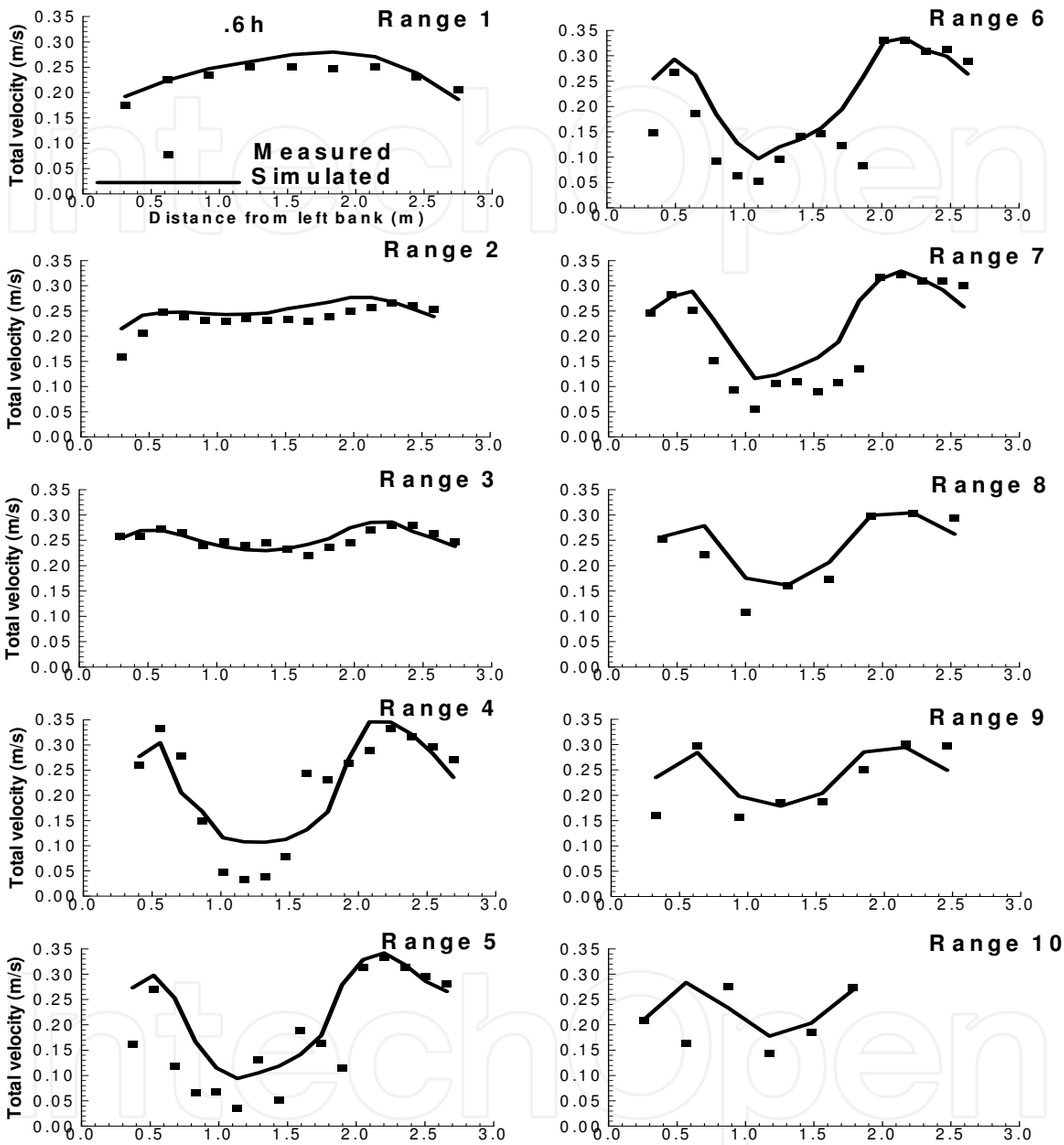


Fig. 4b. Comparison of simulated and measured total flow velocities at 0.6 *h* from the water surface around the submerged weir. Horizontal axis is the distance from the outer bank.

Fig. 4c shows the comparison of measured and computed velocities near the bed. The trend of approaching flow deceleration and separation just upstream of the weir are similar to those at the 0.6 *h* level. Because the front surface of the weir was not vertical, the flow tends to adhere to the sloping surface. No recirculation of horseshoe type was observed. Directly downstream of the weir, the near bed measurement level is in the recirculation zone. Both measured and computed velocities at Range 4 and 5 are negative (downstream direction is defined positive) close to the weir. Further downstream, negative velocities become positive

and increase gradually over the zone of reattachment. The near bed velocity in the thalweg changed direction near the Range 6 and the computed velocities agreed well with those measured. The overall agreement of measured and computed velocities at this level is better than those at the 0.6 *h* level. Since the reattachment occurred along the triangle-shaped edge of the recirculation zone and the measurements were taken along straight lines with relatively large spacing, it is difficult to compare reattachment directly.

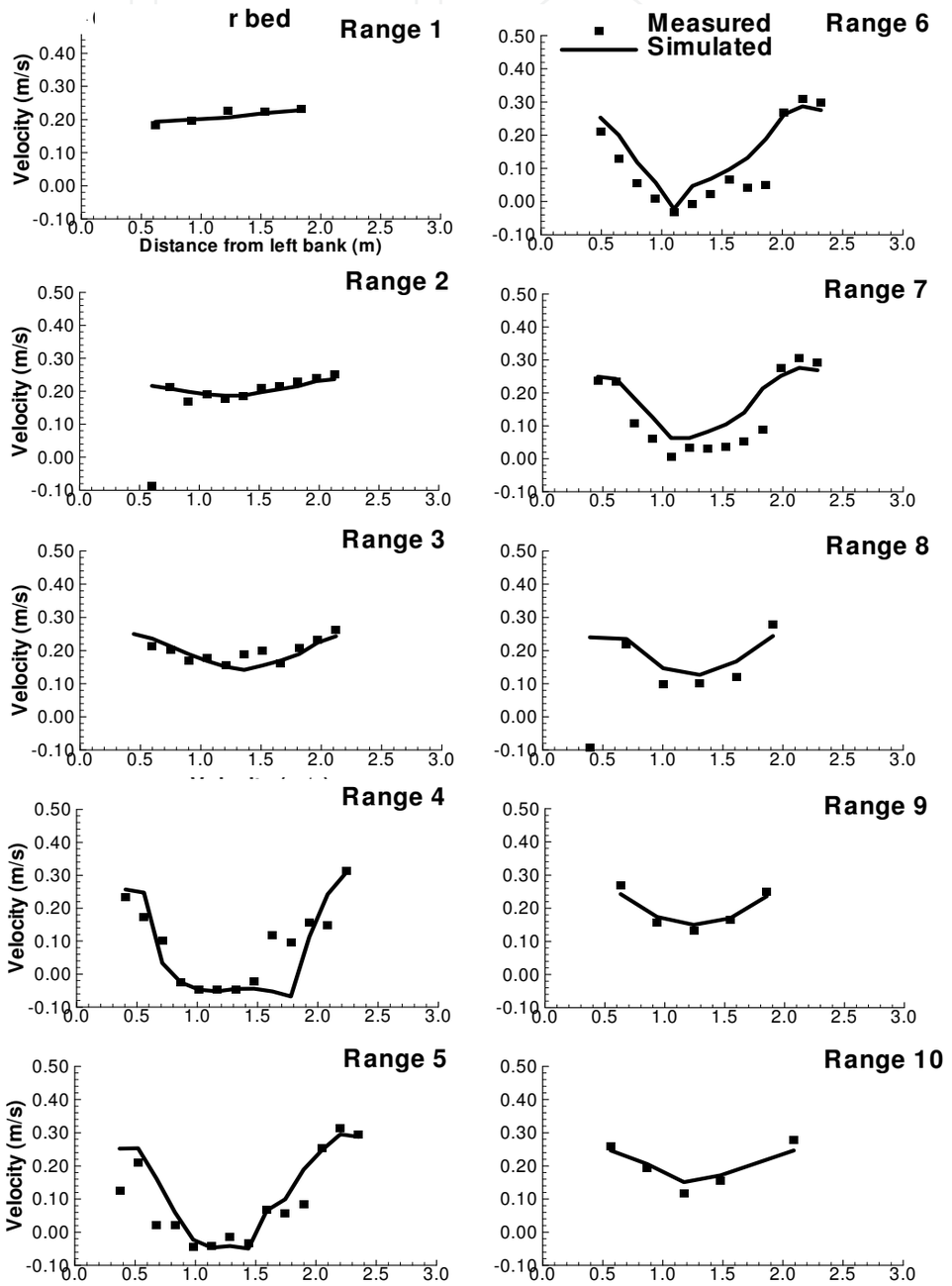


Fig. 4c. Comparison of simulated and measured horizontal flow velocities near the bed around the submerged weir. Horizontal axis is the distance from the outer bank.

### 3.3 Flow structure around a submerged weir

The flow near a submerged weir in a channel bendway is highly three-dimensional and complex. Because the weir is the largest obstacle in the flow path, the flow pattern in the vicinity of the weir is dominated by parameters such as weir length, height, angle, shape and roughness. Fig. 5 shows computed flow (vector) field in the recirculation zone directly behind the weir with the vertical scale enlarged (4x) to enhance clarity. Fig. 5a is the vector pattern near the bed. Fig 5b is a vertical section cut through middle of the circulation. The

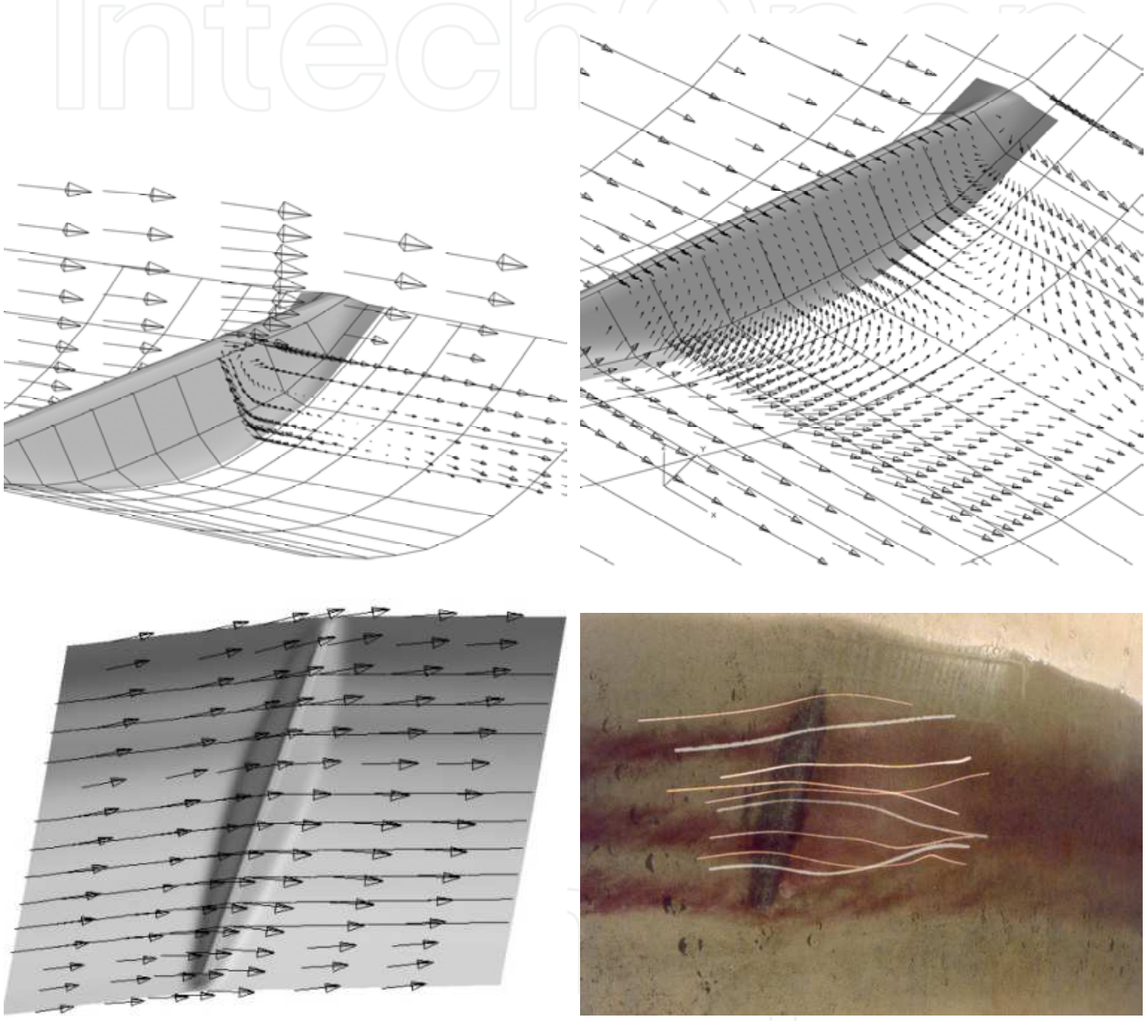

Fig. 5. Vector field of the flow behind the submerged weir (velocity near water surface is about 0.3 m/s). a: computed vectors near the bed; b: computed vectors in a vertical section across the weir; c: computed vectors on the water surface; d: observed confetti trace lines.

flow in the recirculation zone behind the weir is directed backward against the weir and entrained by the shear layer. Fig. 5c shows the flow vectors on the water surface, with some longitudinal mesh lines shown as references. The vectors near the tip of the weir turn to the inner bank while those near the shoulder are toward the outer bank. Apparently, the pattern of a typical helical secondary current in a channel bendway has been altered due to the

presence of the submerged weir. Significant flow velocity change occurs over the top of the weir. Because the water depth over the weir was small, comparable to the size of the ADVP device, velocity measurement over the weir top was difficult. Similarly, the velocities at the flow surface could not be measured. Due to these shortages one was unable to validate the computed secondary flow direction at the surface. Confetti trace lines of the physical model (Fig. 5d) and the particle trace lines released on the water surface level of the computed flow field were compared. The distributions of these trace lines are very similar which indicate the predicted surface velocity directions are consistent with the physical model.

Fig. 6 shows the surface elevation contour lines. A high pressure zone forms at upstream of the weir with a low pressure zone forming just downstream. The well known pattern of water surface superelevation in a bendway is altered significantly due to the presence of the weir. Because the alignment is 20˚ toward upstream, the high pressure zone is located closer to the outer bank and low pressure zone is closer to the tip of the weir and the inner bank. The flow passing the top of the weir inevitably turns toward the inner bank under such a pressure distribution. The pressure skew seems to be the key to understanding why the secondary current near the weir changes direction and become favorable to navigation.

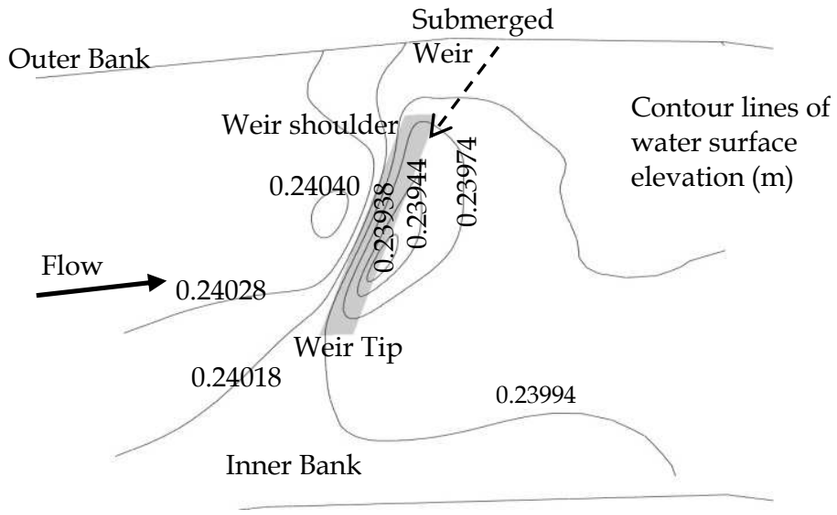


Fig. 6. Pattern of water surface elevation contour (m) near the submerged weir

Summarizing the observations in the physical model and numerical simulation, the flow pattern sketch around a submerged weir is shown in Fig. 7. Upstream of the weir, the high pressure zone slows down the approach flow and tends to force the flow to separate. The general helical secondary flow pattern in the approach channel is thus being changed. The high pressure difference across the weir (shown in Fig. 6) accelerates the flow which tends to pass over the top of the weir perpendicularly and creates a recirculation zone behind the weir near the bottom. This recirculation zone and the overtop flow are separated by a shear layer. Due to the shape of the channel bed, the recirculation zone is approximately triangular. In the deeper portion of the channel, the recirculation enhanced by the shear flow is stronger and requires a longer distance to dissipate. This triangular recirculation zone can be clearly seen in the physical experiments. After the flow has passed the weir, the flow pattern caused by the weir dissipates gradually downstream. The distance to fully recover the flow pattern depends on the flow condition and the weir configuration. This distance is important for determining optimal weir spacing when a multiple weir design is considered.

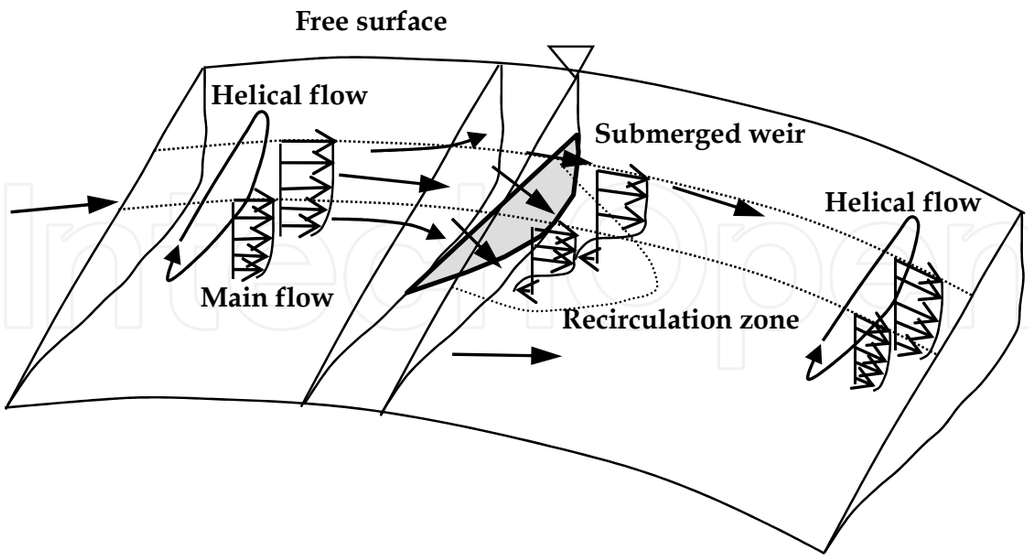


Fig. 7. Flow structure around a submerged weir

### 3.4 Flow field of the helical secondary currents

In order to illustrate secondary flow patterns, the computed flow fields are presented in a series of cross-sections. These cross-sections are aligned in the direction of the radius of curvature; the secondary current was defined as the velocity normal to the main flow direction. The main flow direction was defined as the mean flow direction in the channel without the submerged weir. Additional simulations were conducted to compute the main flow directions for each submerged weir case.

Fig. 8 shows the weir alignment near the bendway apex and the display cross-sections ($J$). All the cross-sections are equally spaced ($\Delta l$) along the centerline. For clarity, the spacing between these sections in the figure was exaggerated. The secondary currents presented in Fig. 9 are from some of these sections.

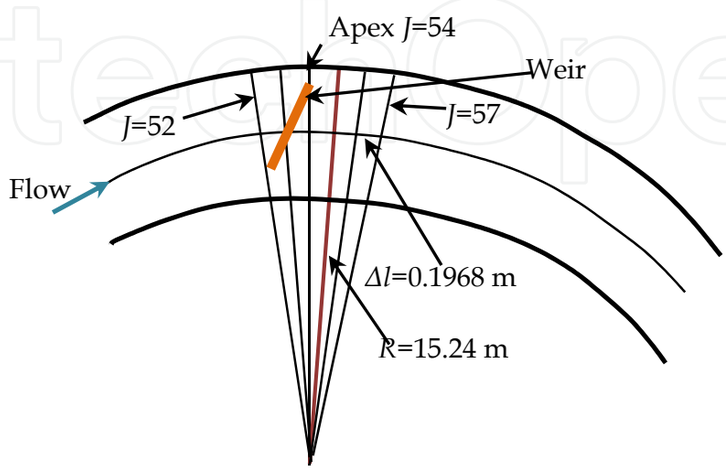


Fig. 8. Sketch of the simulation channel and the display cross-sections

The cross-sections in Fig. 9 are from upstream (Fig. 9a) to downstream (Fig. 9k), with the outer bank on the left and inner bank on the right side. The counter clockwise secondary current shown in section 40 (Fig.9a), far upstream of the SW, is a typical helical flow pattern. Closer to the SW in section 47 (Fig. 9b), the helical structure is altered because the main flow decelerates and separates. Since the weir has an angle of 20$^{o}$ from the radius line, it intercepts with several display sections (Fig. 8). The presence of the SW is reflected by highly complex secondary current and strong vertical motion shown in section 49, 50, 51, 52, (Fig. 9c, 9d, 9e, 9f) which cut across the SW.

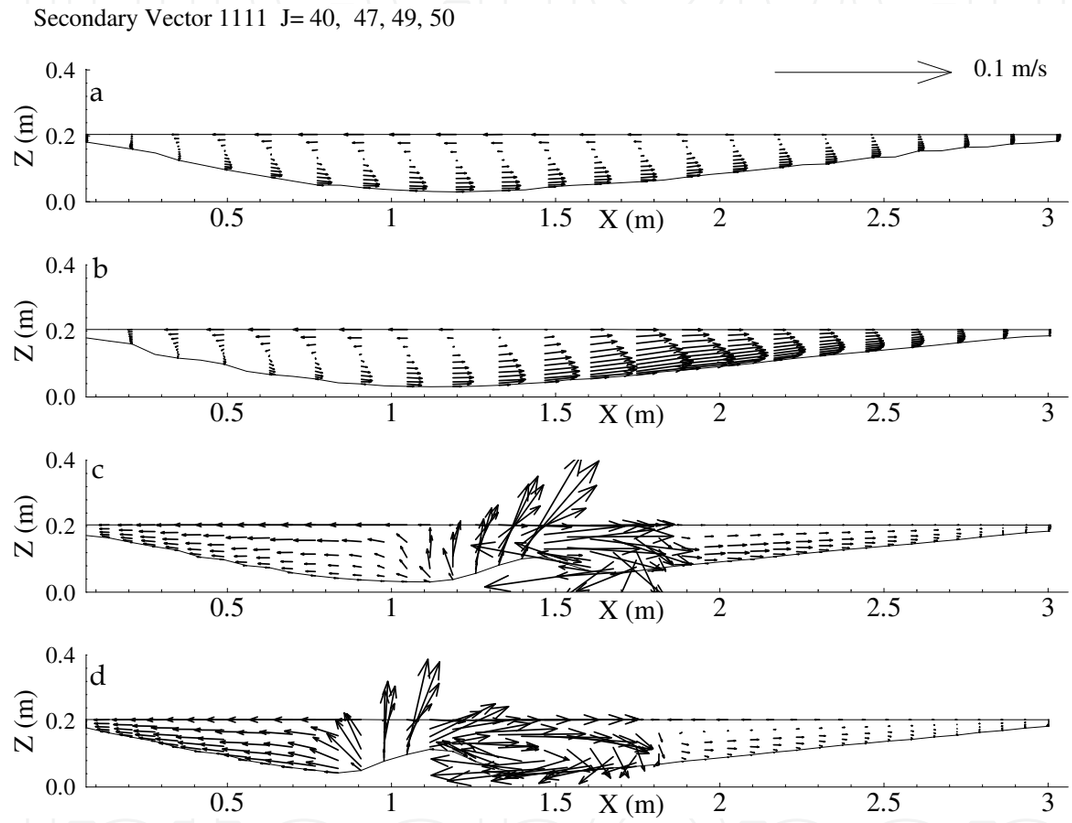


Fig. 9. (a) (b) (c) (d). Secondary current in the approach flow

The single celled, counter-clockwise helical current in the approaching flow becomes three cells behind the weir: the one in the center is strong and has inverse, clockwise direction; the other two near the banks are weaker (Fig. 9g and 9h). The inverse cell appearing on the right side of the weir is actually on the downstream side if one observes a top view of the flow pattern. The inverse cell is strong near the weir and dissipates gradually downstream, indicating that the influence of the weir is in a limited distance. The two cells near the banks are much weaker than the inverse center cell, however, they are of the same direction as that of the helical current in the approach flow. These two concomitant circulations are partly driven by the inverse cell and partly influenced by the flow around the tips of the weir. They gain strength gradually as the inverse cell is dissipated (Sec. 54, 58, 60, 66, Fig 9g, 9h, 9i, 9j). They finally reconnect and form a single helical current cell

across the channel (Sec. 78, Fig. 9k). The helical current will strengthen further downstream until complete recovery.

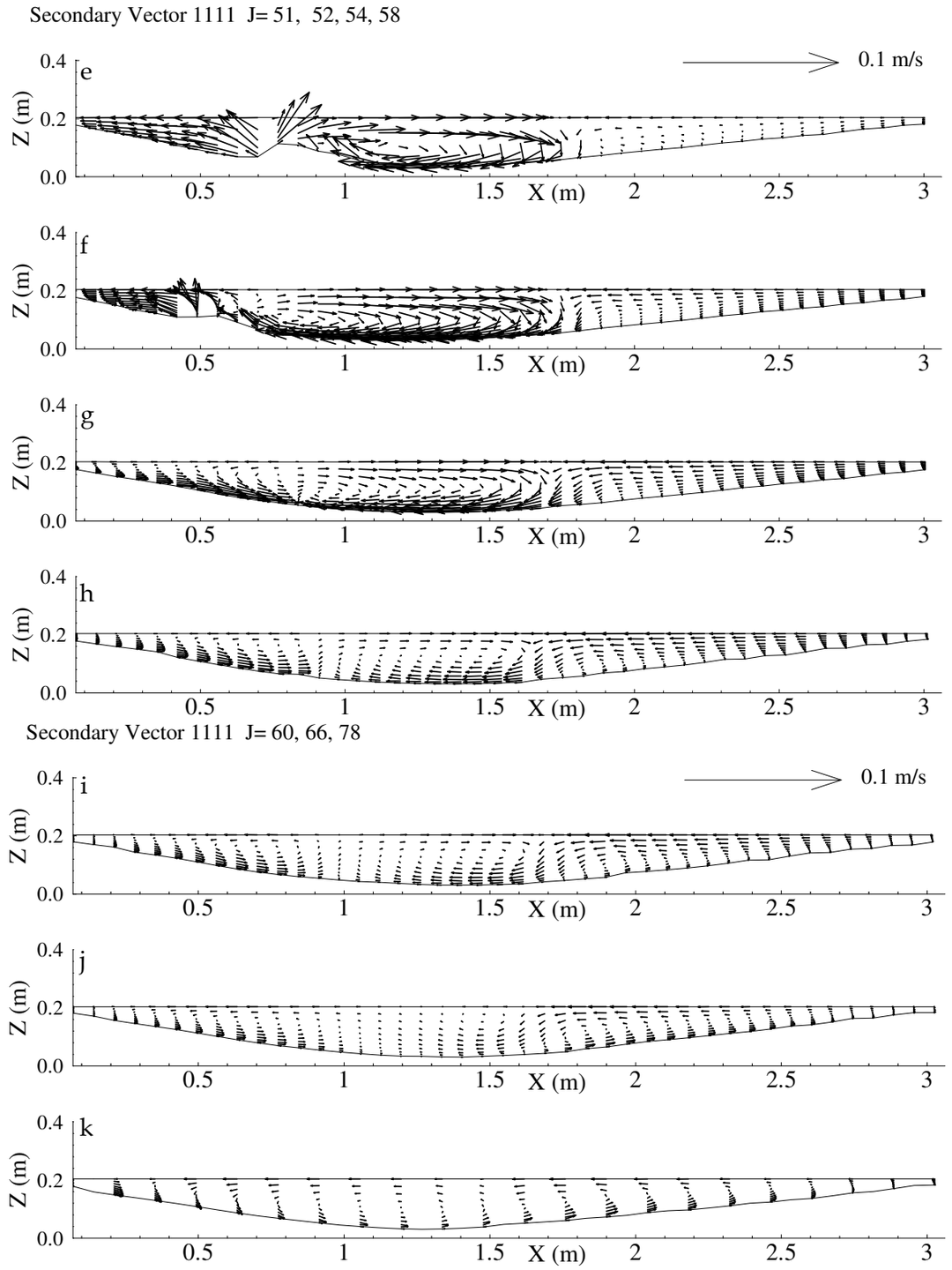


Fig. 9. (e) (f) (g) (h) (i) (j) (k) Secondary flow passing the submerged weir

Because of the inverse flow cell, the flow velocity near the centerline on the water surface is toward the inner bank instead of the outer bank. This cell of secondary flow inverse to the normal helical cell is beneficial to navigation because it cancels the effect of the general helical current and realigns flow toward the inner bank. The foot print of the inverse secondary current on the free surface is an area extending downstream from the SW. The length, width, and location of this realigned area are important to the safety of channel navigation. Since the flow velocity could not be measured close to water surface and the measuring ranges were set near the SW, one could not directly validate the predicted surface flow realignment. More detailed measurements covering the entire zone would be necessary to confirm the numerical results.

## 4. Study of Victoria Bendway

### 4.1 River geomorphology, hydraulic structures and measured velocity data

In 1995, six submerged weirs were constructed on the outer bank of Victoria Bend in the Mississippi River in an attempt to improve navigation conditions (Fig. 10). The effectiveness of submerged weirs on surface flow realignment in Victoria Bendway (VBW) of the Mississippi River was studied.

VBW is located at the confluence of the White River, between the State of Arkansas and Mississippi. The discharge in the Mississippi River upstream of the VBW is influenced by the White River. VBW is a highly curved bend, with a ratio of the radius of curvature to the channel width varying from 1 to 3 approximately, depending on the river stage. It has a $108^{o}$ heading change and a radius of 1280 m. It is expected that the secondary current would be very strong in such a channel, which creates a navigation hazard to navigating barges.

The submerged weirs were oriented upstream with angle from 69 to 76 degrees between the weirs and the bend longitudinal line. Post-construction surveys indicated deposition at the upstream reach of the weir field and scouring throughout the rest of the weir system. Three long spur dikes were constructed on the flood plain or point bar of the VBW. The effect of these dikes is to converge the flow to the main channel, therefore the point bar is protected from erosion, and the channel is re-aligned to enhance navigation.

A comprehensive survey of this reach was conducted by the US Army Corps of Engineers in 1998. The data were measured by acoustic devices with bed elevation referenced to a Cartesian coordinate system. In addition to the bed elevations, velocity data were taken in VBW using Acoustic Doppler Current Profiler instrumentation on June 11 and June 12, 1998. Three velocity transects were taken adjacent to each of the six submerged weirs: one upstream, one downstream, and one over the top of the weirs (Fig. 11). A few transects were taken between weirs with others downstream of the weir field where strong scouring occurred. Because of the highly turbulent flow in the bendway, the surveyed velocity transects were not straight across the channel.

The flow discharge in these two days was about that of a one year return flow and almost constant. The flow depth and width of the channel were large at this discharge with the flow depth in the main channel at about 15-35 m. The depth clearance above the weirs for navigation is about 6 m. The point bar was fully submerged with two of the three dikes partially submerged and the third one (downstream) completely submerged at this flow condition. The discharge was determined by integrating the measured flow flux in transects. Integrations of the flow flux using the measured velocities in each survey path indicate these surveys were quite consistent, resulting in a near constant discharge (~12,600 $m^3/s$) with only a few exceptions.

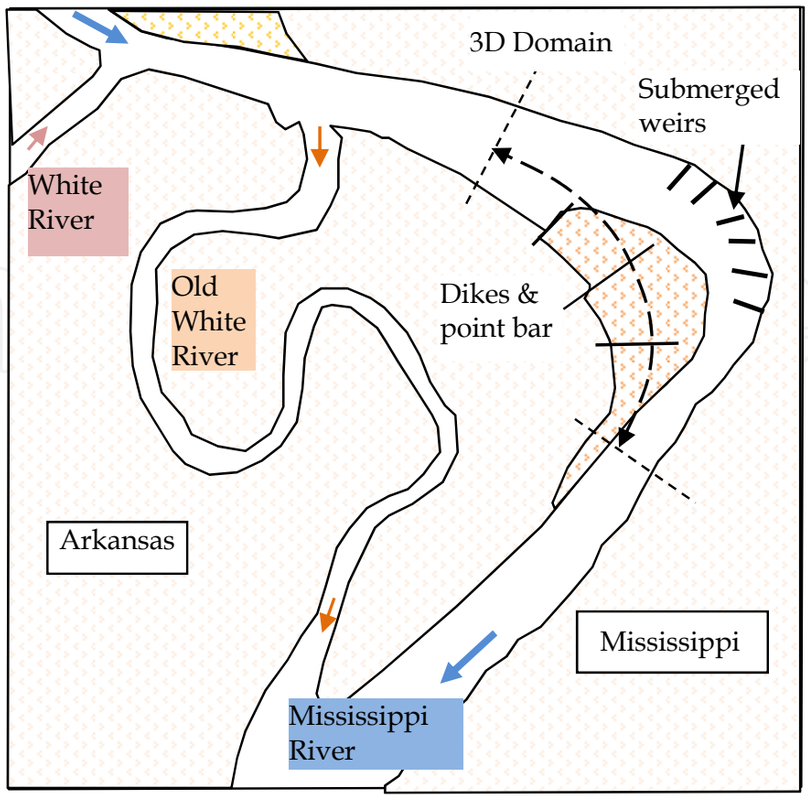


Fig. 10. Victoria Bendway of the Mississippi River, the White River and submerged weirs

Fig. 11 shows the bathymetry of the VBW and the 34 survey transects for measuring the velocity field. The weirs constructed in the main channel are depicted using contours of bed elevation. At each survey point, three-dimensional velocities were obtained along a vertical line at a number of points ranging from 5 to more than 100, depending on the flow depth. The velocity data measured on June 11, have 17 sections with a total of 2210 survey points while the data taken on June 12, include 17 transects with a total of 2494 survey points. Due to turbulent flow and complex bed bathymetry, the transects could not be held straight, particularly at where the point bar and thalweg meet. Actual transects are longer than those shown in Fig. 11, extending from the outer bank onto the point bar. The survey paths shown are the portion in the main channel consisting of about 35% of the total length of transects. Because the beam angle of the ADCP was 20˚, the sampling diameter near the bottom of the main channel (~30 meter deep) would be around 22 meters. This implies that scattering of the data would be large, particularly close to the irregular part of the bed and weirs, and the data may not be able to resolve flow structures in the weir field. Muste et al. (2004) discussed factors influencing the accuracy of ADCP measurement in general and evaluated a particular velocity profile measured in the middle of a straight reach of the Upper Mississippi River (Pool 8 near Brownsville, MN). For a steady flow of 4.5 m deep at the measuring point, sampling duration of 11 minutes were necessary at a fixed point to obtain a stable mean velocity profile. The measured mean velocity could differ as much as 45% if the sampling duration was less than 7 minutes. Since the flow velocity in the VBW was stronger and the flow depth larger, the measured mean velocity therefore could have a larger error because the survey vessel was moving continuously and the data was obtained

by averaging signals sampled in a short distance. The average time for measuring one transect of the VBW was about 10 minutes and that for a point was a few seconds. The velocities measured at the surface level often have large differences from those measured at lower levels, due to perhaps the influence from navigation traffic in the river, the survey vessel, or limitations of the measuring instrumentation.

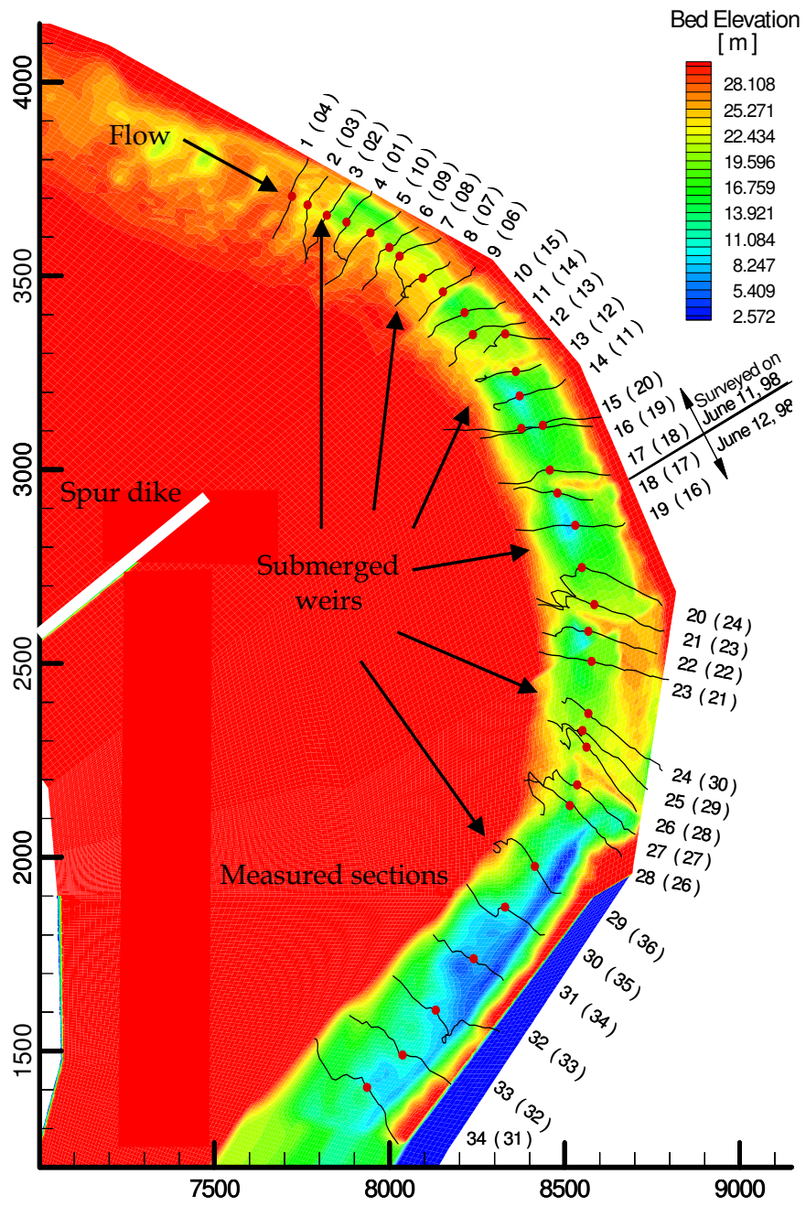


Fig. 11. Bed bathymetry, submerged weirs and the survey paths in the main channel. Section numbers are marked along the outer bank.

There was a large elevation difference between the main channel bed and the point bar, particularly near the downstream of the bendway. The weir field has caused additional

deposition and erosion at the upstream and downstream channel of the bendway, respectively. The bed between the weirs was also severely scoured. The resistance of the weir field would slow down the approach flow, stimulate deposition and cause additional flow toward point bar. The scouring in and downstream the weir field may result from additional turbulence due to the weirs and the reduced sediment load in the flow.
The approach of this study is to apply the 3D numerical model validated using experiment data to simulate the flow and evaluate the effectiveness of weirs. The numerical solutions provide a much higher resolution of the flow field and make it possible to resolve more detailed flow around the submerged weirs. The field velocity measurements were used to validate again the three-dimensional flow model. Comparison of the simulations for the pre- and post-weir channel revealed the effect of the weirs on the flow pattern.

### 4.2 Numerical simulation and model validation

Although the three-dimensional velocity data obtained were very detailed, the resolution of the three survey transects adjacent to a weir were not sufficient for analyzing the near field flow and its effect on navigation. Because the river channel near the Victoria Bendway was at the confluence with the White River, the channel pattern was complicated (Fig. 10). In order to use available computational resources efficiently, the 3D simulation was limited to a short bendway reach with a curved computational domain of 4.6 km along the main channel and 1.8 km wide in the apex section. A two-dimensional model (CCHE2D, Jia & Wang 1999; Jia et al., 2002a) was used to simulate a much longer reach (a 33.866 km stretch) to calibrate the resistance parameter and to establish initial flow, upstream and downstream boundary conditions for the 3D simulation. The effective roughness heights of the channel were obtained by calibration using measured water surface elevation along the channel. This roughness was used for the 3D simulation with the exception of the surface roughness of the SW. It was approximated to be one half of the gravel of which it was constructed. The upstream flow boundary conditions for the 3D model (flow rate and direction distributions) were specified with the 2D model results. The depth-averaged velocity at each point of the boundary of the 3D domain was converted to a logarithmic profile and no secondary flow was imposed since the inlet boundary was located in a relatively straight portion of the channel (Fig. 10).
The extended 2D channel stretches upstream and downstream of the VBW with a mesh size of 123 (transversal) x 622 (longitudinal); more than 50% of the horizontal mesh nodes were in the range of the bendway where 3D computations were carried out. The 3D computation is for the flow in the bend with a mesh of 123 (transversal) x 322 (longitudinal) x 11 (vertical); more vertical mesh points were located near the bed. Three 3D grids ($G_1$:58x189x8, $G_2$:123x322x11, and $G_3$:123x324x14) were tested. Using the three meshes, the RMS error of the simulation results and the measured data were computed and indicated in Table 2. Non-dimensional $\sigma_u$ and $\sigma_v$ are for the $u$ and $v$ velocity component, respectively. Computational points in the domain are much more than those measured. RMS errors were computed using measured data and computational results interpolated to the measuring point. The error of simulations is considerably less in the upper part of the flow (less than 8 m from the surface) than that in the lower part (deeper than 8 m from surface). The accuracy of the simulations did not significantly improve when mesh resolution was increased. As was mentioned earlier the scatter of the ADCP data was quite large particularly near the bed. This is attributed to larger data scatter near the bed such that the numerical accuracy improvement due to mesh refinement was much smaller than the data scattering.

| Mesh | No. of vertical points | Zone of calculation | $\sigma_u / U_{mean}$ | $\sigma_v / U_{mean}$ |
|---|---|---|---|---|
| $G_1$ | 8 | Upper profile | 0.219 | 0.269 |
| | | Lower profile | 0.363 | 0.34 |
| $G_2$ | 11 | Upper profile | 0.218 | 0.262 |
| | | Lower profile | 0.36 | 0.336 |
| $G_3$ | 14 | Upper profile | 0.220 | 0.269 |
| | | Lower profile | 0.36 | 0.337 |

$U_{mean}$~1.4 m/s is the mean velocity for the entire reach. Upper profile is the water surface to the 8 meters deep point, Lower profile is from the point to the bed.

Table 2. RMS error of the data and simulation results using three meshes

The mesh size of $G_2$ in the main channel ranges from 12 to 30 m, approximately. A submerged weir was resolved by 15 to 20 grid points. The submerged weirs are the largest resistance elements in the main channel. The back side slope of the weirs observed from the bed topography is less than 15˚. The largest weir in the bendway was about 230 m long and 10 m high. The first weir upstream was hardly visible due to significant deposition in front of the weir.

2D simulation was used as a tool to calibrate roughness of the channel. The calibrated Manning's coefficient $n$=0.037 is reasonable considering large scale of bed forms, the number of structures (dikes, submerged weirs) built in this channel reach. Water stage data on June 11, 1998, from five gauge stations along the reach of 2D simulation, were used for the calibration. The calibrated Manning's coefficient was then transformed to equivalent roughness height for the three-dimensional model by using Strickler's function

$$n = \frac{d^{1/6}}{A} \tag{11}$$

where $A$ is an empirical constant which may represent both grain and form resistance ($A$=19 according to Chien and Wan, 1999), and $d$ (~0.121 m) is the effective roughness height which is consistent with a large data set for the Mississippi River (van Rijn, 1989). Graf (1998) showed that $A$ could vary from 20 to 45 in rivers with cobble or gravel bed. The effective roughness is used in the wall function for specifying hydraulic rough boundary condition:

$$\frac{u_0}{u_*} = \frac{1}{\kappa}\ln(\frac{z}{z_0}) \quad \text{for} \quad \frac{u_* k_s}{\nu} > 70 \tag{12}$$

$$z_0 = 0.03 k_s$$

where $u_o$ is the near bed flow velocity, $u_*$ is shear velocity, $\kappa$ (=0.41) is the Karman's Constant, $z$ is the distance from a wall, $\nu$ is the fluid viscosity and $k_s$ (~$d$) is the roughness height. Although roughness height can be converted from the Darcy-Weisbach factor, Chezy's coefficient or Manning's coefficient more rigorously (van Rijn, 1989), Eq. 11 was used for its simplicity. Since $d$ was a calibrated parameter, it lumps many factors related to the resistance such as bed forms and grain roughness. The three point-bar dikes are large

and resolved by the 2D model. The area of the submerged weir field was less than two percent of the 2D simulation domain; the effective roughness height thus evaluated was affected by the weir field only slightly. Measurement of bed form in the Mississippi River (Leclair, 2004) revealed that the size of dunes ranges from 120 to 11 m with height ranges from 3 to 1 m; dune length near a bendway is about 69 m. Considering the mesh size of the main channel (12-30 m), the bedforms were not resolved by the model. Therefore, it is reasonable to model their resistance using a lumped effective roughness height, and the computational grid was considered being over the roughness elements (Wu et al., 2000). The mixing length and $k$-$\varepsilon$ turbulence closure schemes were applied in this study. Results indicate that the solutions from these two schemes had no significant differences in terms of defining the main and helical flow. Bed roughness varies spatially in the channel and the effective roughness used was a constant calibrated according to water surface profile.

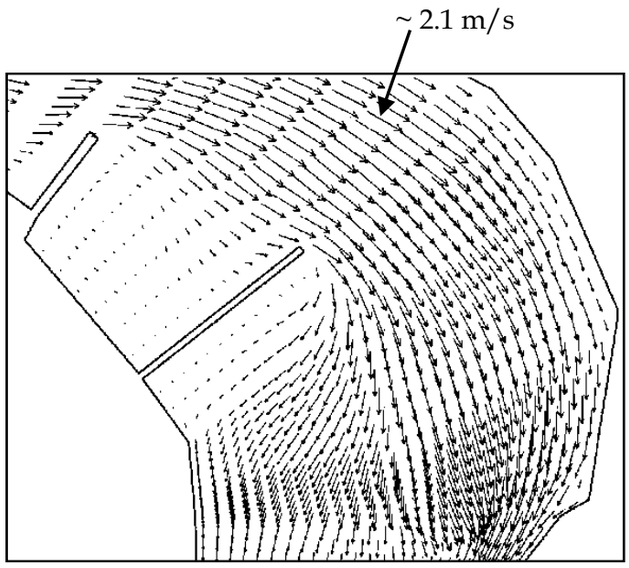


Fig. 12. Simulated flow pattern (velocity m/s) near water surface in Victoria Bendway

Fig. 12 demonstrates the simulated flow field near the free surface of the channel. For clarity, the resolution (velocity points) shown is only a few percent of the original. The first and second dikes on the point bar were submerged only slightly. They were treated as un-submerged in the simulation. A large area of recirculation was present between the first and second long spur dikes, with the recirculation lengths limited by the dike spacing. The recirculation behind the second dike was limited closely behind it and small in size, due to channel curvature. One can also observe the flow pattern from the point bar returning to the main channel near the end of the bendway.

Contour lines of surface velocity magnitude on the background of bed elevation shading are shown in Fig. 13. The river stage was high with the point bar and the third dike on the right bank submerged. One can see the flow velocity variation along the channel due to the existence of the second dike and weir structures. Because the water depth was less over the submerged weirs, the flow accelerates over the weirs.

Fig. 14 shows the computed water surface elevation contour overlaying the image of bed elevation. More contour lines are concentrated near the weir and show a similar pattern: the contour lines align parallel to the weirs and widen near the tips of the weirs. This distribution

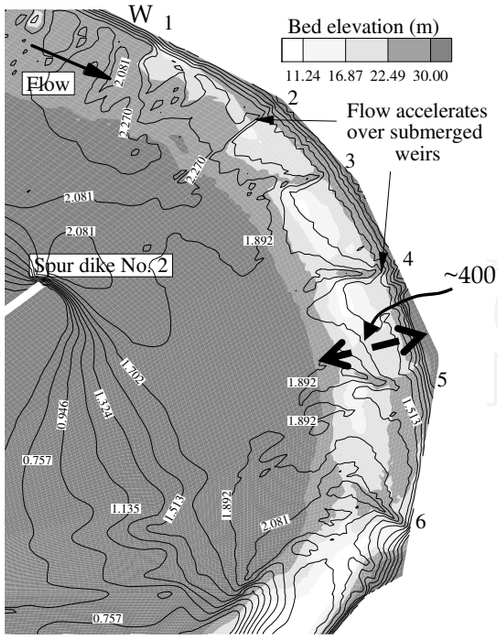


Fig. 13. Simulated distribution of velocity magnitude (m/s) near the water surface level

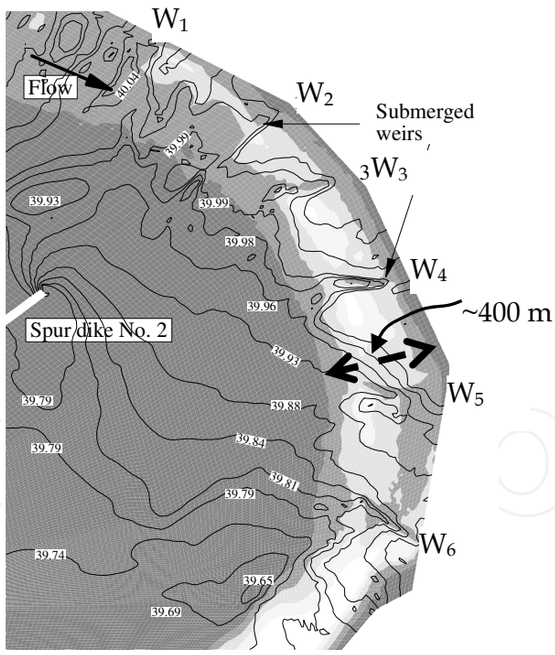


Fig. 14. Water surface elevation contours (m) in the main channel with submerged weirs

would accelerate the flow over the weir top normally and tends to turn the flow toward the inside of the bend. The helical current due to channel curvature is toward the outer bank; therefore, such a surface elevation pattern resulting from the submerged weirs reduces the strength of the helical current. In Fig. 6, the simulated surface elevation contours for the experiment case was also aligned parallel to the weir, similar to this field case; although due

to the difference in channel bathymetry, flow depth, and weir size relative to channel, etc., the patterns of the simulated water surface in these two cases are not exactly the same. However, the paralleled contours produce pressure gradients perpendicular to the weirs and thus help improving navigation.

To evaluate the quality of numerical simulations, model validation was performed by comparing the simulation and the measured 3D velocity data. Because the computational mesh points were different from those of the velocity survey, one has to interpolate the numerical solution to the 3D survey points. Inverse distance interpolation was used to compute the velocity from the eight vortices of a hexahedral mesh cell containing a measuring point.

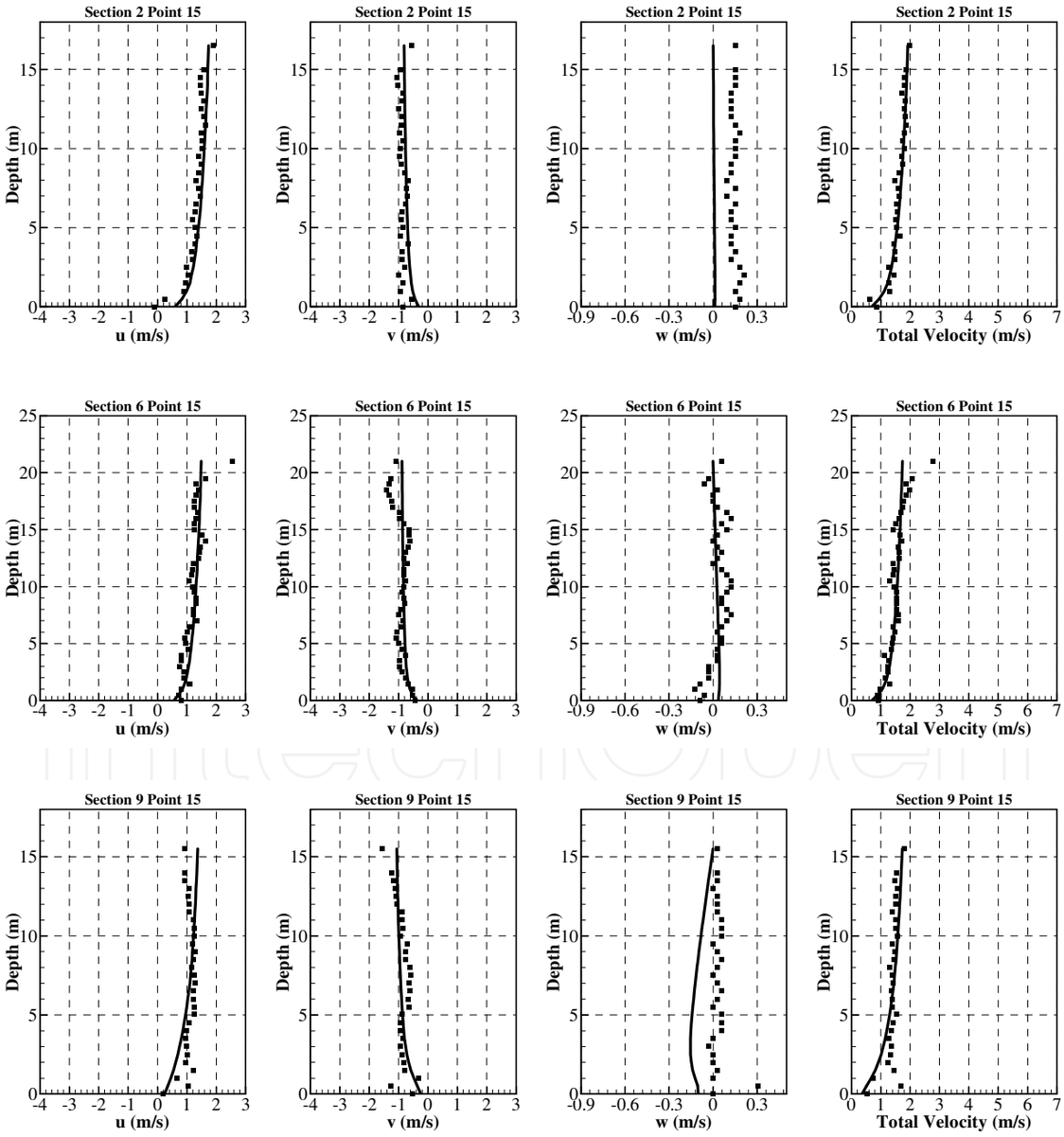

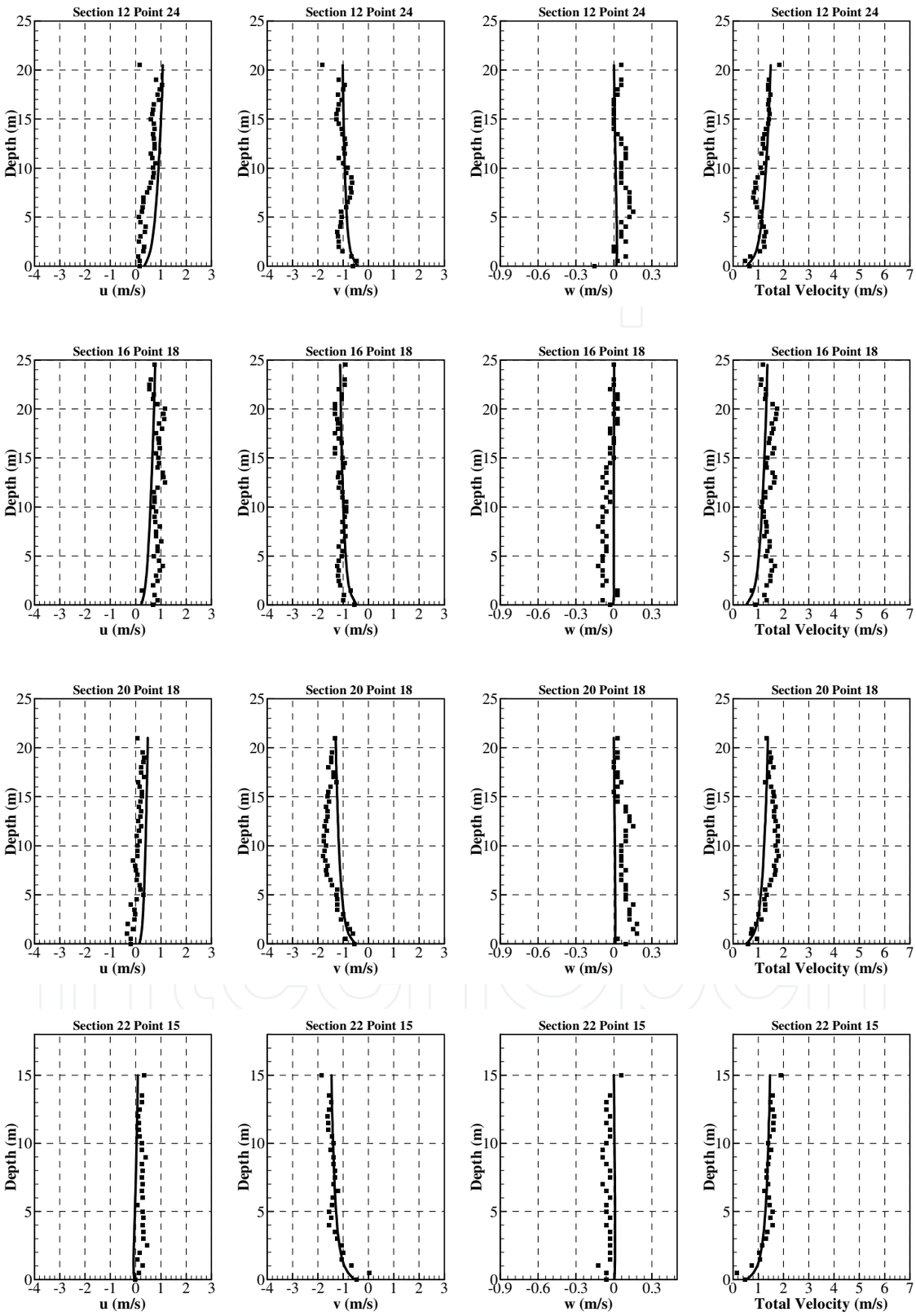
Section 12 Point 24
Depth (m)
u (m/s)
Section 12 Point 24
Depth (m)
v (m/s)
Section 12 Point 24
Depth (m)
w (m/s)
Section 12 Point 24
Depth (m)
Total Velocity (m/s)
Section 16 Point 18
Depth (m)
u (m/s)
Section 16 Point 18
Depth (m)
v (m/s)
Section 16 Point 18
Depth (m)
w (m/s)
Section 16 Point 18
Depth (m)
Total Velocity (m/s)
Section 20 Point 18
Depth (m)
u (m/s)
Section 20 Point 18
Depth (m)
v (m/s)
Section 20 Point 18
Depth (m)
w (m/s)
Section 20 Point 18
Depth (m)
Total Velocity (m/s)
Section 22 Point 15
Depth (m)
u (m/s)
Section 22 Point 15
Depth (m)
v (m/s)
Section 22 Point 15
Depth (m)
w (m/s)
Section 22 Point 15
Depth (m)
Total Velocity (m/s)

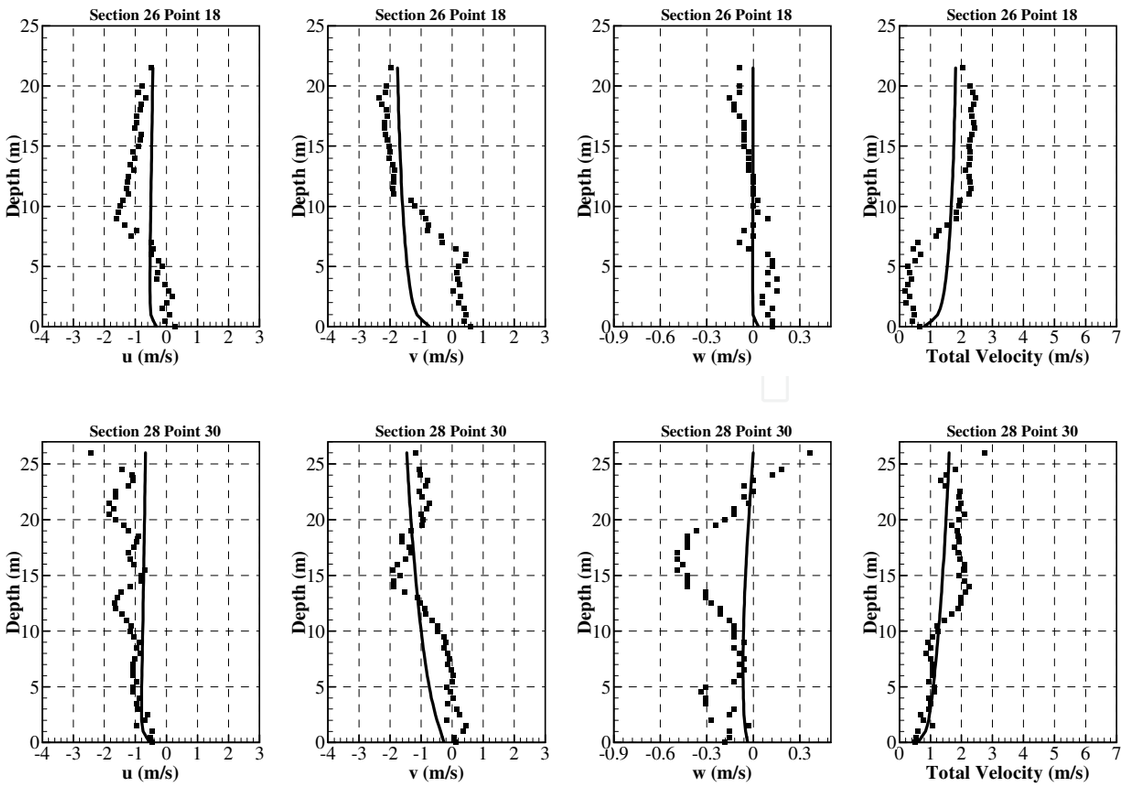


Fig. 15. Comparisons of computed and measured velocity profiles, along the main channel, Victoria Bendway

Because there were more than 4500 survey points, it is impossible and unnecessary to show all the comparisons. Instead, only a limited number of points are presented. Several vertical profiles are selected along the main channel (Fig. 11). Some points are located in scour holes between weirs, and others are very close to the weirs. Fig. 15 shows comparisons of these velocity profiles. Along each profile, computed and measured velocity components $u$, $v$, $w$ and total velocity are compared. The depth of the flow at these survey points ranges from less than 20 m to about 35 m. Results indicate that the computed velocity profiles are smooth curves in most areas of the channel, with the velocity magnitude increasing toward water surface. Most of the comparisons show adequate agreement between data and simulation, particularly in trend. The agreement is generally better for points away from the weirs. No recirculation zone was found behind the weirs in the field data. In general, measured data show scatter and variation along vertical lines and transects, and the scatters appear to be random. For example, at measuring point 30 of Section 28, the measured velocities indicate stronger variations along the vertical. Distributions like this are often located either near abrupt bed change or close to a weir. At these locations, turbulence would be very strong and the upper and lower portion of the flow may have different directions. Simulating a mean turbulent flow, the numerical model resulted in a much smoother flow field than the measured velocities taken in highly turbulent and unsteady natural conditions.

Fig. 16 shows the computed and measured velocity magnitude at ten selected transects. Comparisons at three levels $0.05h$, $0.4h$ and $0.8h$ (from the bed to water surface) are

presented. One finds general agreements along each level and section. The data scatter near the channel bed is, in general, greater than in the upper portion of the water column, consistent with the RMS errors indicated in Table 2, which could be resulted from the large near-bed sampling volume of the ADCP and complex channel topography. The comparisons were performed for the main channel rather than the point bar, because the main interest of this study was the flow characteristics in the main channel. Although the differences between the computed and measured data are large for many points, the trend of the numerical results generally agrees with the data, particularly near the free surface (0.8*h*). These comparisons (Fig. 15 and Fig. 16) have confirmed the consistency of the numerical model with the field data and its applicability to this particular problem.

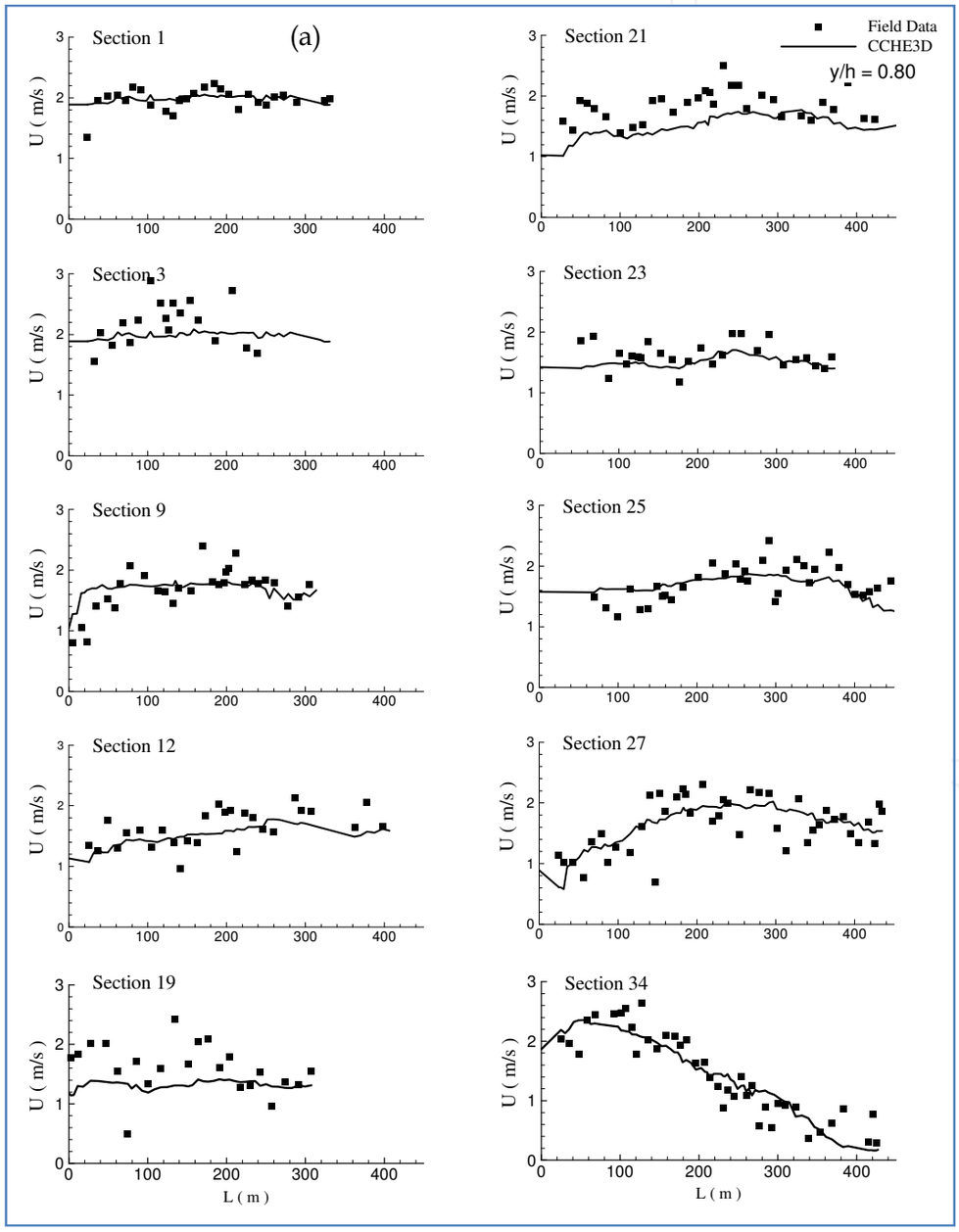

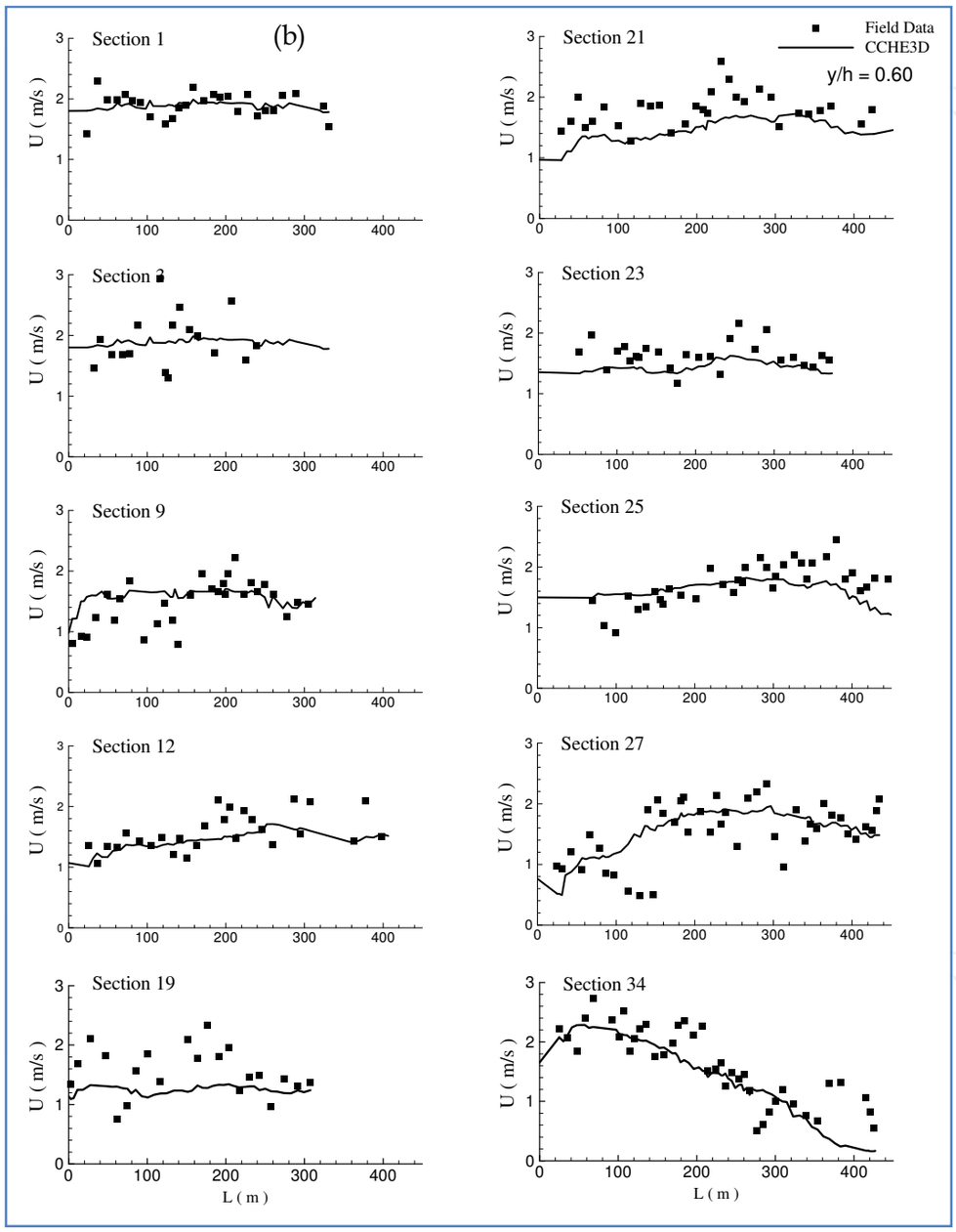
(b)
Field Data
CCHE3D
y/h = 0.60
Section 1
Section 21
Section 3
Section 23
Section 9
Section 25
Section 12
Section 27
Section 19
Section 34
U ( m/s )
L ( m )

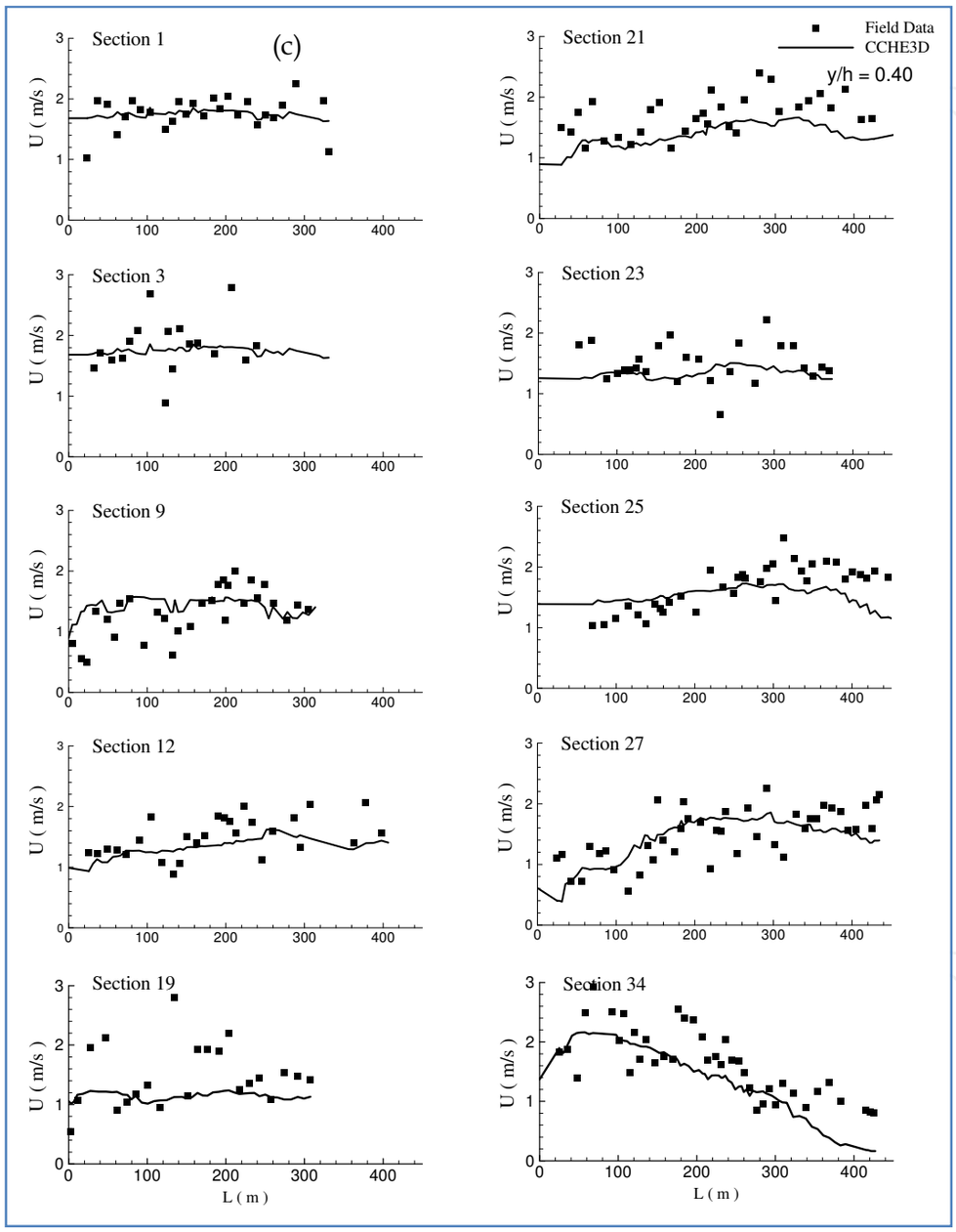
(c)
Field Data
CCHE3D
y/h = 0.40
Section 1
Section 21
Section 3
Section 23
Section 9
Section 25
Section 12
Section 27
Section 19
Section 34
U ( m/s )
L ( m )

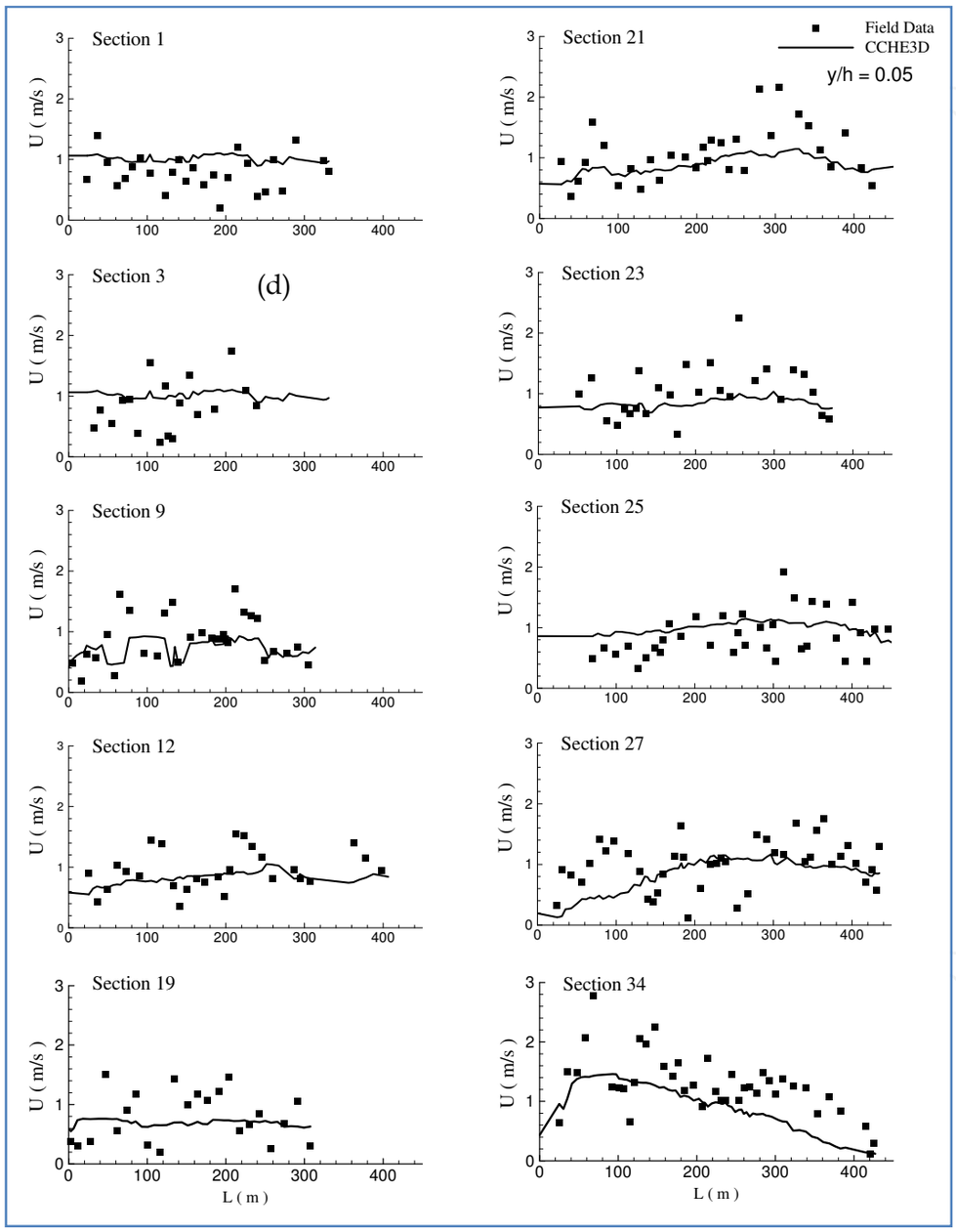


Fig. 16. Comparison of computed and measured flow velocity at selected sections (a) near water surface (z/h=0.8); (b) near middle depth (z/h=0.6); (c) near middle depth (z/h=0.4); and (d) near bed (z/h=0.05).

### 4.3 Helical secondary current and submerged weirs

Fig. 17 shows a plan view of the simulated 3D flow and comparison of computed and measured secondary flows in a transect. Vectors (in red) at surface level (Fig. 17a) are plotted with those near the bed (in black). The difference in their directions at each point represents the helical current. For clarity, only a limited number of vectors are shown.

Looking upstream, the main helical current in the main channel is clockwise. The secondary flow near the tip of the spur dike is also clockwise, but has been weakened or even reversed at some locations. Since it does not follow the channel curvature, the flow over the point bar goes directly into the main channel and alters the main flow there.

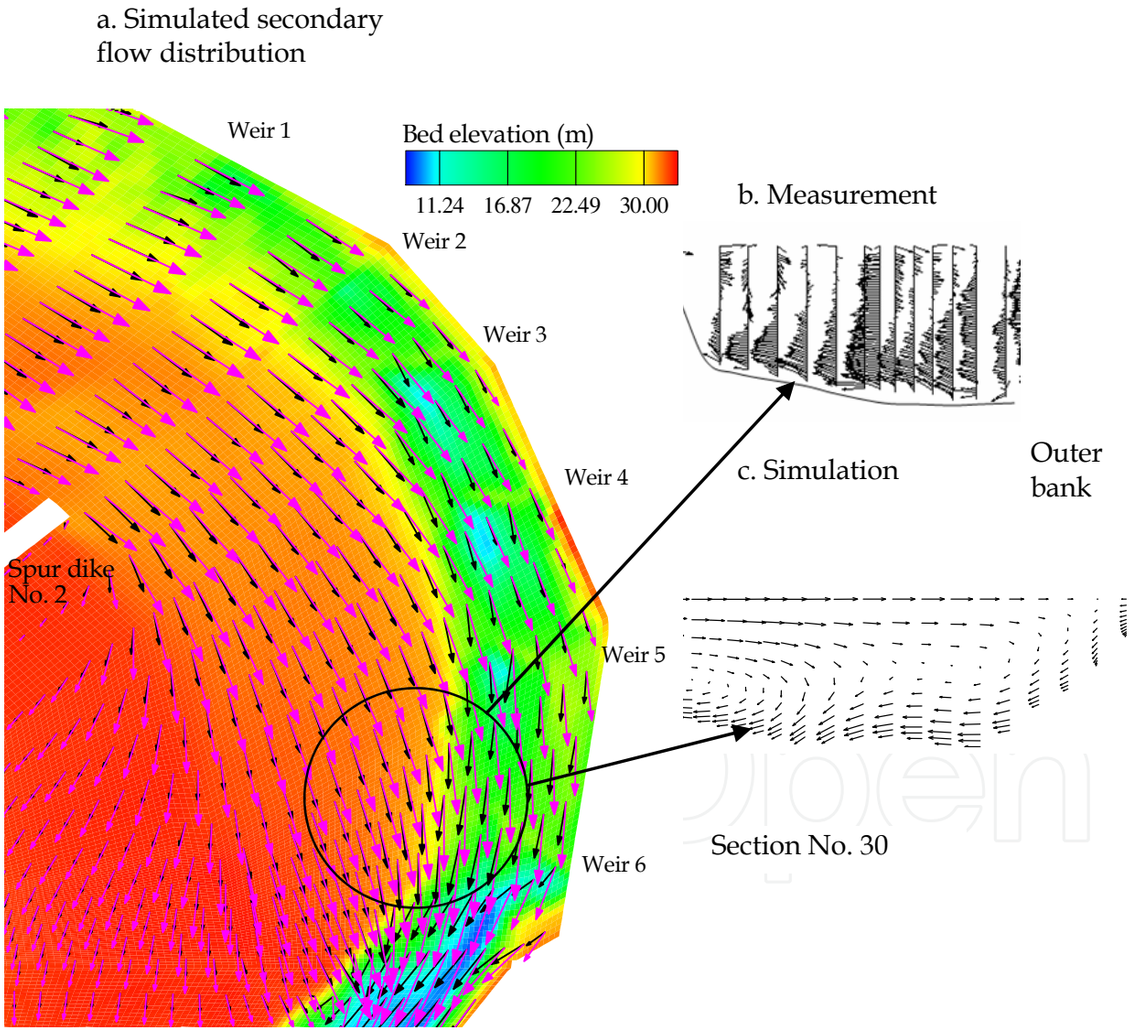


Fig. 17. Simulated secondary helical current in the bendway. a) General flow pattern; b) Measured secondary velocity in the main channel near the point bar; and c) Computed secondary velocity in the main channel near the point bar.

The flow over the point bar starts to converge back to the main channel at the downstream port of the bend. The returning flow near the edge of the point bar is not parallel to the edge; the component normal to the main flow affects secondary current in the main channel. With this particular bendway morphology configuration, the flow from the point bar back to the main channel tends to enhance the helical current. Since the main channel deepens near the 6th SW, a large bed elevation step appears between the point bar and the main channel. Affected by the flow from the point bar, the secondary current in the main channel appears to be intensified (around survey section 30, Fig. 11), as indicated by measurement (Fig. 17b) and simulation (Fig. 17c). The influence on the channel flow is similar to those observed by Sellin (1995) and by Shiono & Muko (1998) in their experiments in which the flow from a flood plain affects the secondary flow in the main channel. This indicates that the helical flow in the main channel is strengthened, consistent with the observation that severe channel erosion occurs on the downstream portion of the bend.

## 5. Influence of submerged weirs on navigation in VBW

Navigation problems in bendways are mainly attributed to the helical secondary current which tends to push vessels toward the outer bank (the inertial and centrifugal forcing due to the vessel's own motion are not considered). The simulated secondary flows with and without the submerged weirs were compared to assess the effectiveness of these weirs in reducing the strength of the secondary flow. The submerged weirs were removed from the computational domain; the deposition and erosion patterns, due to the presence of the weirs, were corrected using the channel bathymetry (cross-sections) surveyed in 1994 before the weir field installation as a reference. A 2D simulation was also conducted for producing boundary conditions.

The influence of the submerged weirs on the helical current was evaluated by the difference in the secondary current with and without weirs. Fig. 18a shows the computed secondary current in sections upstream, over, and downstream submerged weir No. 4. The orientation of these sections was approximately normal to the main flow direction. The secondary flow is strongly changed by this submerged weir. In the section over the weir, the changes in the secondary flows are dramatic. Near the water surface, the transversal flow toward the outer bank is reduced or reversed. Because vessels in bendways are pushed laterally by the transverse flow, this submerged weir effect would be beneficial to the channel navigation. In sections between weirs, the secondary current tends to recover the normal pattern of curved channel flows. Fig. 18b shows the computed helical current in the corresponding sections without the submerged weir.

The direction of the near surface flow defined by the angle

$$\theta = \arctan \frac{u_{transversal}}{u_{longitudinal}} \tag{14}$$

was used as an indicator of the flow alignment or navigation condition in bendways. If the angle ($\theta$) is very small, the navigation condition is considered good because the flow would be aligned more along the main channel. To evaluate how the weir system influenced the flow angle, the difference of the flow angle at the free surface in the main channel with and without weirs, $\Delta\theta$ (= $\theta_{\text{with weirs}}$ - $\theta_{\text{without weirs}}$) was computed and presented in Fig. 19. Considering the secondary flow is normally in the order of $0.1u_{longitudinal}$, or less, the change of flow angle in the order of 5.7 degree would be sufficient to cancel the near surface secondary velocity.

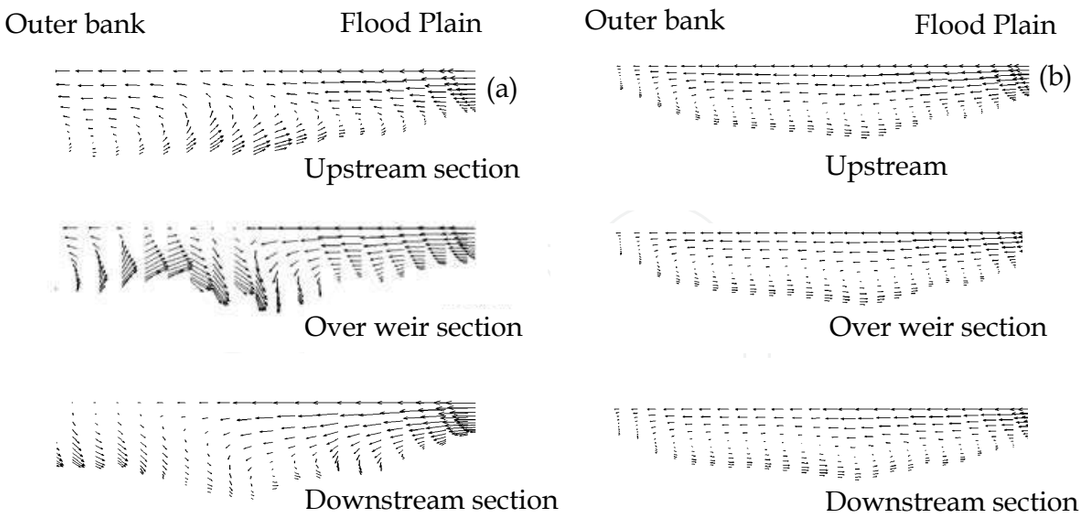


Fig. 18. Secondary currents around submerged weir No. 4; a) with weirs, b) without weirs

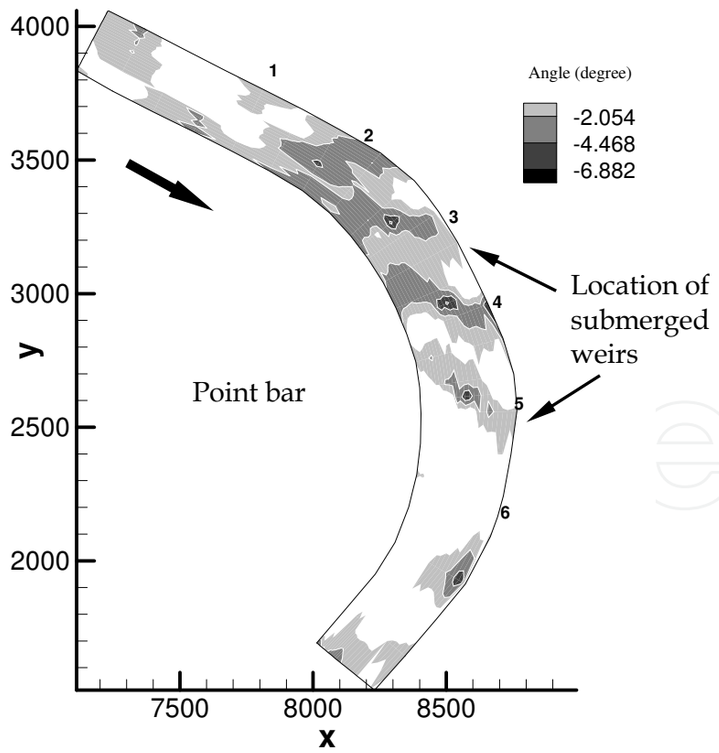


Fig. 19. The difference of the flow angles between the flows with and without submerged weirs. Only the main channel is shown. The portion with improved condition (with negative $\Delta\theta$) is shaded.

The areas with a negative angle represent where the flow condition is improved, whereas the areas with a positive value indicate where the condition became worse. To distinguish the areas with an improved condition, the contours of the area with a worsened condition is replaced with white. It is seen that the total improved area is larger than 50% and that conditions are better near the weirs. The flow angle change is high over the weir tops and low between them. The maximum angle change reaches about 6.8˚ with less change between weirs. The flow condition near weir No. 6 is worsened, because the strong flow from the point bar returns to the main channel and the secondary current intensifies. After the construction of the weirs, the resistance of the main channel increased resulting in more water flowing over the point bar at the entrance of the bend and then returning to the main channel. The strength of the secondary current near weir No. 6 is thus increased (Fig. 17). The excessive deposition upstream of the weir field in the main channel has disabled the first weir; thus, the first weir is not functional (Fig. 19). In addition, the first and last weir were angled less than others, so they should be less effective even without the influence of the flow from the point bar and sedimentation. To a certain extent, a weir would be more effective if it is angled more toward upstream; its effect on realigning the flow is also influenced by relative length, relative depth, and channel curvature, etc. (Jia et al., 2002b). Future submerged weir designs should consider the influence of local morphology (flood plain). Since the influence of the weirs varies in terms of water depth and relative weir height, additional studies with several more flow conditions are necessary to enhance submerged weir designs.

## 6. Conclusions

A three-dimensional computational model for free surface turbulent flows, CCHE3D, has been applied to study flows in bendways affected by submerged weirs. Both experimental data and field data were used for model validation. The flow distribution due to a weir in a bendway was discussed and the effect of multiple weirs in the Victoria Bendway in the Mississippi River on channel navigation was studied. The comparisons showed good agreement in both the experiment and field cases between measured and simulated data which confirmed the consistency of the numerical model, the physical model and the large scale field case.

The general helical secondary current pattern in the experimental channel was disturbed by the single weir, particularly in its vicinity. In the experiments with a submerged single weir, it was found that the weir resulted in a high pressure zone forming on its upstream side and a low pressure zone on the downstream side. The high pressure zone slows the approaching flow and tends to separate it, forcing more flow toward the ends of the weir with the velocities near the tips increasing and higher than in the center region of the weir and the channel. The low pressure behind the weir creates a triangle-shaped recirculation zone. Due to the alignment of the weir (angled toward upstream), the high pressure and the low pressure zones are not located along the general stream direction. The high pressure zone is located closer to the outer bank and the low pressure zone is closer to the inner bank (tip of the weir). The skewed distribution tends to realign the overtopping flow toward the inner bank, which is opposite to the general helical current direction. The realigned surface current and the recirculation behind the weir form an inverse secondary cell. Two weaker secondary cells along the banks were also observed parallel to the inverse cell.

Due to the submerged weir, the flow velocity near the center of the experimental channel decreases and that near the tips of the weir increases. These high velocity zones may result in bed erosion and channel widening. The contours of the water surface are parallel to the weir direction and surface flow direction was realigned to the inner bank, thus being favorable to navigation. The effect of the weir is limited, and normal curved channel flow pattern may recover downstream. Further research is necessary to quantify sediment transport characteristics of bendways containing submerged weir fields.

In Victoria Bendway with multiple weirs, the simulation indicated that the helical current was only significant in the main channel. The flow over the point bar has little curvature and secondary current structure under the flow conditions studied is very weak. The helical current in the main channel was enhanced by the flow returning back to the main channel from the point bar.

For the case of Victoria Bendway, the computed velocities were smooth curves varying in the vertical direction, while the measured velocities show scatters much larger than the experiment case. Because of the nature of the ADCP instrument, the scatters are particularly strong near the bed, in close vicinity of weirs, and where the main channel and point bar join. A larger discrepancy of velocity comparisons would appear in these areas. The comparisons along measured transects at several vertical levels show reasonable agreement with the best agreement appearing near the water surface (0.8*h*).

In the main channel of Victoria Bendway, the direction and magnitude of the secondary current were affected by the submerged weirs. Not only was the secondary current structure changed, the secondary flow near the free surface around the weirs was weakened. This is consistent with the simulated water surface elevation pattern which tends to realign the flow over the top of the weirs. The way the flow is affected by these weirs is similar to that observed in the experimental channel of the physical model.

To study the overall effectiveness of the weir field, numerical simulations without weirs were also carried out and the solutions were compared to that with weirs in Victoria Bendway. Flow direction change in the main channel was compared and the weir effectiveness was evaluated. Most of the weirs (four out of six) were found effective, but the first and last weir were not. The ineffectiveness was caused by the channel deposition and the flow returning from the point bar enhanced the helical current. In addition, a smaller alignment angle made them less effective.

## 7. Acknowledgement

This investigation was conducted under contract agreement No. DACW42-01-P-0243 and No. DACW42-00-P-0456 with the US Army Corps of Engineers, Waterways Experimental Station, and the National Center for Computational Hydroscience and Engineering, The University of Mississippi. Professor Pierre Julien of Colorado State University provided valuable suggestions in reviewing a part of this study. Mr. Michael F. Winkler of USACE provided the physical model data. The authors appreciate the help of Dr. Yaoxin Zhang at NCCHE for his technical assistance.

## 8. References

Bhuiyan, A.B.M.F. & Hey, R.D. (2001). Instream J-vane for bank protection and river restoration, *XXIX IAHR Congress Proceedings*, Beijing, China. Theme D, Vol. II, pp 161-166.

Bhuiyan, F & Olsen, N.R.B., (2002). Three-dimensional numerical modeling of flow and scour around spur-dikes, *Proceedings of the Fifth International Conference on Hydroinformatics,* Cardiff, UK, 2002, 70-75

Blanckaert, K. & Graf, W.H. (2001). Mean flow and turbulence in open-channel bend, *J. Hydraulic Eng.*, 127(10), 835-847.

Booij, R. (2003). Modeling the flow in curved tidal channels and rivers, *Proceedings, International Conference on Estuaries and Coasts,* Nov. 11, 2003, Hangzhou, China, pp786-794.

Chien, N. & Wan, Z. (1999). *Mechanics of Sediment Transport*, ASCE press, ASCE, 1801 Alexander Bell Drive, Reston, Virginia 20191-4400.

Davinroy, R. D. & Redington, S.L. (1996). Bendway weirs on the Mississippi River, a status report, *Proceedings of the 6th Federal Interagency Sedimentation Conference*, March 10-14, 1996, Las Vegas, NV, pp III32-37.

De Vriend, D.J. (1979). *Flow measurements in a Curved Rectangular Channel*, Laboratory of Fluid Mechanics, Department of Civil Engineering, Delft University of Technology, Internal Report No. 9-79.

Duan J.G., Wang, S.S.Y., & Jia, Y. (2001). The application of the enhanced CCHE2D model to study the alluvial channel migration processes, *J. Hydraul. Res.*, 39(5) 2001, 469-480.

Graf, W.H. (1998). *Fluvial Hydraulics*, John Willey & Sons Ltd, Baffins Lane, Chichester, West Sussex PO19 1UD, England.

Hsieh, T.Y. & Yang, J.C. (2003). Investigation of the suitability of two-dimensional depth-averaged models for bend flow simulation, *J. Hydraul. Eng.,* 129(8), 597-612.

Jarrahzade, F. & Bejestan, M.S. (2011). Comparison of maximum scour depth in Bank line and nose of submerged weirs in a sharp bend, *Scientific Research and Essays,* Vol. 6(5), pp. 1071-1076, 4 March, 2011, available online at http://www.academicjournals.org/SRE

Jia, Y., & Wang, S.S.Y. (1992). Computational model verification test case using flume data, *Proceedings: Hydraulic Eng.,* 436-441, ASCE.

Jia, Y., & Wang, S.S.Y. (1993). 3D Numerical Simulation of Flow Near a Spur Dike, *Advances in HydroScience and Engineering*, *Proceedings of International Conference for Hydroscience and Engineering,* Vol. I Part B, pp2150-2156. University of Mississippi, June, 1993.

Jia, Y & Wang, S.S.Y. (1999). Numerical model for channel flow and morphological change studies, *J. Hydraul. Eng.*, ASCE, 125(9), 924-933.

Jia, Y., & Wang, S.S.Y. (2000a). Numerical Study of Turbulent Flow around Submerged Spur Dikes, *2000 International Conference of Hydroscience and Engineering*, Korea.

Jia, Y., & Wang, S.S.Y. (2000b). Numerical simulations of the channel flow with submerged weirs in Victoria Bendway, Mississippi River, *Technical Report No. NCCHE-TR-2000-3*, National Center for Computational Hydroscience and Engineering, The University of Mississippi.

Jia, Y., Blanckaert, K., & Wang, S.S.Y. (2001a). Simulation of secondary flow in curved channels, *Proceedings of the FMTM2001 International Conference*, Tokyo, Japan.

Jia, Y., Kitamura, T., & Wang, S.S.Y. (2001b). Simulation of scour process in plunging pool of loose bed-material, ASCE, *J. Hydraul. Eng.*, 127(3), 219-229.

Jia, Y., Wang, S.Y.Y., & Xu, Y. (2002a). Validation and application of a 2D model to channels with complex geometry, *International Journal of Computational Engineering Science*, 3(1) (March 2002), 57-71.

Jia, Y., Wang, S.S.Y., Xu, Y., & Huang, S.L. (2002b). Research on Optimal Parameters of Submerged Weirs Using Numerical Simulation and Physical Model Data, *Technical Report TR-2003-2,* National Center for Computational Hydroscience and Engineering, The University of Mississippi.

Jia, Y., Scott, S., Xu, Y.C., Huang, S.L., & Wang, S.S.Y. (2005). Three-Dimensional Numerical Simulation and Analysis of Flows around a Submerged Weir in a Channel Bendway, *J. Hydraulic Eng.*, 131(8), 682-693, August 1, 2005.

Jia, Y., Scott, S., Xu, Y.C., & Wang, S.S.Y. (2009). Numerical Study of Flow Affected by Bendway Weirs in Victoria Bendway, the Mississippi River, *Journal of Hydraulic Engineering*, 135(11), ASCE, p902–916.

Kuhnle, R., Jia, Y., & Alonso, C. (2002). 3-Dimensional Measured and Simulated Flow for Scour Near Spur Dikes, *First International Conference on Scour of Foundations, ICSF-1*, Texas A&M University, College Station, Texas, USA, November 17-20, 2002, Vol.1 349-363.

Jin, Y.C. & Steffler, P.M. (1993). Predicting flow in curved open channels by depth-averaged model, *J. Hydraul. Eng.*, ASCE, 119(1), 109-124.

Kinzli, K.D. & Thornton, C.I. (2010). Predicting velocity in bendway eddy fields, *River Res. Applic.* 26: 823–834 (2010), DOI: 10.1002/rra.1289

Lai, Y.G., Weber, L.J., & Patel, V.C. (2003). Nonhydrostatic three-dimensional model for hydraulic flow simulation, I: formulation and verification, *J. Hydraul. Eng*. 129(3), 196-205.

Leclair, S.F. (2004). Multi-scale dunes of the Mississippi River: the analysis of time variation of probability distributions of bed elevation as s step toward the understanding of bed load sediment transport, *Denver Annual Meeting (November 7-10, 2004), Paper No. 198-8*, Geological Society of America, Abstract with Programs, Vol. 36, No. 5, p. 461

Leschziner, M.A. & Rodi, W. (1979). Calculation of strongly Curved Open Channel Flow, *J. Hydraulics Division*, ASCE, 105(10), 1297-1313.

Martin, S. K & Luong, P.V. (2010). Analyzing shoaling reduction techniques on the Atchafalaya River at Morgan City, LA, *2nd Joint Federal Interagency Conference*, Las Vegas, NV, June 27 - July 1, 2010.

Mayerle, R., Toro, F.M., & Wang, S.S.Y. (1995). Verification of a three dimensional numerical model simulation of the flow in vicinity of spur dikes, *J. Hydraul. Res.*, 33(2), 243-256.

Morvan, H., Pender, G., Wright, N.G., & Ervine, D.A. (2002). Three-dimensional hydrodynamics of meandering compound channels, *J. Hydraul. Eng.*, 128(7), 674-682.

Muste, M., Yu, K., Pratt, T., & Abraham, D. (2004). Practical aspects of ADCP data use for quantification of mean river flow characteristics; Part II: fixed vessel measurements, *Flow Measurement and Instrumentation*, 15 (2004) 17-28.

Nezu, I., & Nakagawa, H. (1993). *Turbulence in Open Channel Flows*, A.A. Balkema, Rotterdam, Netherlands.

Odgaard, A.J. & Kennedy, J.F. (1983). River-bend bank protection by submerged vanes, *J. Hydraulic Eng.*, ASCE, 109(8), 1161-1173.

Olsen, N.R.B. (2003). Three-dimensional CFD modeling of self-forming meandering channel, *J. Hydraul. Eng*., 129(5), 366-372.

Olsen N.R.B. & Stokseth S. (1995). Three-dimensional numerical modelling of water flow in a river with large bed roughness, *Journal of Hydraulic Research* 33: 571–581.

Ouillon, S. & Dartus, D. (1997). Three-dimensional computation of flow around groyne, *J. Hydraulic Eng.*, ASCE, 123(11), 962-970.

Rajaratnam, N. & Nwachukwu, B.A. (1983). Flow Near Groin-Like Structure, *J. Hydraul. Eng.*, ASCE, 109(3), 463-480.

Rozovskii, I.L. (1961). *Flow of Water In Bends Of Open Channels*, Academy of Science of the Ukrainian SSR, Institute of Hydrology and Hydraulic Engineering, The Israel program for Scientific Translations.

Sellin, R.H.J., (1995). Hydraulic performance of a skewed two-stage flood channel, *J. Hydraulic Res*., 30 (1), 43-64.

Shiono, K. & Muto Y. (1998). Complex flow mechanisms in compound meandering channels with over bank flow, *Journal of Fluid Mechanics*, 376, 221-261.

Speziale, C. G. (1987). On nonlinear *k-l* and *k-ε* models of turbulence, *J. Fluid Mech.*, 178, 459-475.

Stone, H. L. (1968). Iterative solution of implicit approximation of multidimensional partial differential equations, *SIAM Journal on Numerical Analysis*, 5, 530-558.

van Rijn, L.C., (1989). *Handbook: Sediment Transport by Currents and Waves*, Delft Hydraulics, Report H 461.

Wang Sam S.Y. & Hu, K.K. (1992). Improved methodology for formulating finite-element hydrodynamic models, In T.J. Chung, (ed) *Finite Elements in Fluids*, Volume 8, Hemisphere Publication Cooperation, pp457-478.

Wang, S.S.Y., Roche, P.J., Schmalz, R.A., Jia, Y. & Smith, P.E. (ed.) (2008). *Verification and Validation of 3D Free-Surface Flow Models*, American Society of Civil Engineering.

Waterway Simulation Technology, Inc. (1999). A physical model test plan for bend way weir design criteria, *Project summary report to the Navigation Branch of the Coastal and Hydraulics Laboratory*, Waterway Experiment Station.

Waterway Simulation Technology, Inc. (2002). Physical model test for bendway weir design criteria, US Army Corps of Engineers, Engineer Research and Development Center, *ERDC/CHL TR-02-28*, October 2002.

Wilson, C.A.M.E., Boxall, J.B., Guymer, I. & Olsen, N.R.B. (2003). Validation of a three-dimensional numerical code in the simulation of pseudo-meandering flows, *J. Hydraul. Eng*. 129(10), 758-768.

Wu W.M., Rodi W. & Wenka T. (2000). 3D Numerical Modeling of Flow and Sediment Transport in Open Channels, *J. Hydraulic Eng.*, ASCE 126 (1) 4-15.

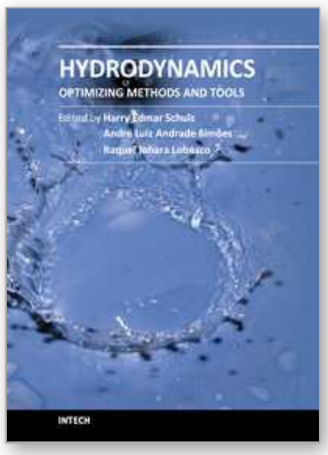


**Hydrodynamics - Optimizing Methods and Tools**
Edited by Prof. Harry Schulz

ISBN 978-953-307-712-3
Hard cover, 420 pages
**Publisher** InTech
**Published online** 26, October, 2011
**Published in print edition** October, 2011

The constant evolution of the calculation capacity of the modern computers implies in a permanent effort to adjust the existing numerical codes, or to create new codes following new points of view, aiming to adequately simulate fluid flows and the related transport of physical properties. Additionally, the continuous improving of laboratory devices and equipment, which allow to record and measure fluid flows with a higher degree of details, induces to elaborate specific experiments, in order to shed light in unsolved aspects of the phenomena related to these flows. This volume presents conclusions about different aspects of calculated and observed flows, discussing the tools used in the analyses. It contains eighteen chapters, organized in four sections: 1) Smoothed Spheres, 2) Models and Codes in Fluid Dynamics, 3) Complex Hydraulic Engineering Applications, 4) Hydrodynamics and Heat/Mass Transfer. The chapters present results directed to the optimization of the methods and tools of Hydrodynamics.

**How to reference**
In order to correctly reference this scholarly work, feel free to copy and paste the following:

Yafei Jia, Tingting Zhu and Steve Scott (2011). Turbulent Flow Around Submerged Bendway Weirs and Its Influence on Channel Navigation, Hydrodynamics - Optimizing Methods and Tools, Prof. Harry Schulz (Ed.), ISBN: 978-953-307-712-3, InTech, Available from: http://www.intechopen.com/books/hydrodynamics-optimizing-methods-and-tools/turbulent-flow-around-submerged-bendway-weirs-and-its-influence-on-channel-navigation

INTECH
open science | open minds

**InTech Europe**
University Campus STeP Ri
Slavka Krautzeka 83/A
51000 Rijeka, Croatia
Phone: +385 (51) 770 447
Fax: +385 (51) 686 166
www.intechopen.com

**InTech China**
Unit 405, Office Block, Hotel Equatorial Shanghai
No.65, Yan An Road (West), Shanghai, 200040, China
中国上海市延安西路65号上海国际贵都大饭店办公楼405单元
Phone: +86-21-62489820
Fax: +86-21-62489821

IntechOpen